

A Modular Programmable Inorganic Cluster Discovery Robot for the Discovery and Synthesis of Polyoxometalates

Daniel S. Salley, Graham A. Keenan, De-Liang Long, Nicola Bell, Leroy Cronin*

School of Chemistry, The University of Glasgow, Glasgow G12 8QQ (UK); email lee.cronin@glasgow.ac.uk

ABSTRACT: The exploration of complex multi-component chemical reactions leading to new clusters, where discovery requires both molecular self-assembly and crystallization, is a major challenge. This is because the systematic approach required for an experimental search is limited when the number of parameters in a chemical space becomes too large, restricting both exploration, and reproducibility. Herein, we present a synthetic strategy to systematically search a very large set of potential reactions, using an inexpensive, high-throughput platform; modular in terms of both hardware and software, and capable of running multiple reactions with in-line analysis; for the automation of inorganic and materials chemistry. The platform has been used to explore several inorganic chemical spaces to discover new, and reproduce known, tungsten-based, mixed transition-metal polyoxometalate clusters, giving a digital code allowing the easy repeat synthesis of the clusters. Among the many species identified in this work, most significantly is the discovery of a novel, purely inorganic $\text{W}_{24}\text{Fe}^{\text{III}}$ -superoxide cluster formed under ambient conditions. The Modular Wheel Platform (MWP) was then employed to undertake two chemical space explorations producing compounds [1-4]: $(\text{C}_2\text{H}_8\text{N})_{10}\text{Na}_2[\text{H}_6\text{Fe}(\text{O}_2)\text{W}_{24}\text{O}_{82}(\text{H}_2\text{O})_{25}]$ (1, {W₂₄Fe}), $(\text{C}_2\text{H}_8\text{N})_{72}\text{Na}_{16}[\text{H}_{16}\text{Co}_8\text{W}_{200}\text{O}_{660}(\text{H}_2\text{O})_{40}]$ (2, {W₂₀₀Co₈}), $(\text{C}_2\text{H}_8\text{N})_{72}\text{Na}_{16}[\text{H}_{16}\text{Ni}_8\text{W}_{200}\text{O}_{660}(\text{H}_2\text{O})_{40}]$ (3, {W₂₀₀Ni₈}) and $(\text{C}_2\text{H}_8\text{N})_{14}[\text{H}_{26}\text{W}_{34}\text{V}_4\text{O}_{130}]$ (4, {W₃₄V₄}), along with many other known species, for example simple Keggin clusters and 1D {W₁₁M²⁺} chains.

Introduction

Exploring the self-assembly and synthesis of high-nuclearity inorganic clusters is challenging as many new chemical procedures are not always reproducible, and the new compounds are often produced in a very low yield.¹ Automation offers a solution allowing digital control of liquid handling as a function of the reaction methodology. Indeed, automated reactor platforms have been used for the synthesis of nanoparticles,² clusters³ and porous materials.⁴ Despite this, an ongoing challenge is to design automated arrays of experiments to allow both the exploration and understanding of the chemical space.⁵⁻⁷ As such, the use of a multiplexed approach to sample large compositional arrays (LCAs) is a valuable strategy since it allows rapid exploration and identification of potential discovery areas in a digital, and reproducible manner. Molecular metal oxides or polyoxometalates (POMs) are one such family of inorganic clusters with nuclearities ranging from 6 to over 360 metal centres. POMs are traditionally formed by group 5 or 6 transition metals (V, Nb, Ta, Mo, and W) in their highest oxidation states; typically synthesized in one pot and purified via crystallization.⁸ POMs have attracted great attention in recent decades for their unique structural properties⁹ and potential application in a number of fields including medicine¹⁰, catalysis¹¹ and materials chemistry¹². More recently, examples of POMs being used as high-density electron storage media have been reported revealing potential use for these compounds in the growing global need for easily accessible energy storage¹³. By combining metal-oxo moieties with heteroanions, such as SO_4^{2-} , PO_4^{3-} , AsO_4^{3-} and transition metal ions, such as Co^{2+} , Fe^{3+} etc.; the stability and structural diversity of the clusters is increased.¹⁴ These units can then be linked by transition hetero-metals (M), such as Co, V, Ni, Mn and Fe allowing building blocks (BBs) with unique structural features to be formed.^{9,15} Furthermore we have recently shown that the exploration of crystallization can be done using active-learning with automated systems, opening up the prospect of developing intelligent search systems exploring supramolecular chemistry.¹⁶

Automation is ideal for the one-pot synthetic procedure involved in most POM synthesis however there are currently only two options available to the chemist when automating any process. First, to incur significant expense by purchasing proprietary hardware and software; or second, to create bespoke technology that can often expire in its utility at the end of the project, despite having required significant resources and expertise to create, test and implement. To provide a more accessible alternative we sought to create an inexpensive, modular device capable of performing the basic tasks needed for simple to moderate-complexity laboratory work. Herein we describe the development of a modular parallelised reactor platform and its application to explore inorganic parameter space efficiently and reliably leading to the discovery of new clusters using digital code. Importantly, the digitization of the search process allowed for highly accurate monitoring of the reaction parameters which led to these discoveries, allowing for consistent repeatability and subsequent optimization. This is vital as newly discovered structural motifs are often isolated in low yield with only a narrow window of ‘synthetic coordinates’. Using this automated platform, we have identified 3 new mixed transition metal W species and the reproducible synthesis of $\{W_{200}Co_8\}$, the largest W-based POM known, built of four $\{W_{49}M\}$ ($M = Co, Ni$) fragments each bridged, in a wheel-like structure, by one $\{WO_6\}$ and one $\{MO_6\}$ unit. This structure in particular is difficult to synthesis and so seemed an appropriate challenge for the platform as part of the project. Each of these compounds were isolated by crystallization, and most importantly, could be readily reproduced using our modular wheel platform.

Results and Discussion

Platform Design

The Modular Wheel Platform (MWP) presented herein is a liquid handling device that uses a combination of custom designed parts (either 3D printed or fabricated in-house), commercially available components and in-house, open-source software; full details for reproduction of which are provided in the SI. Our

platform design allows for addition and modification of functions as needed and was used, in this instance, to explore inorganic chemical space in a high-throughput and reproducible manner. Figure 1 outlines the abstraction of the processes needed for this chemistry (**A**), in addition to the platform's hardware (**B**) and software (**C**). In general, inorganic synthesis space can be traversed by modification of reagents used, relative ratios, concentration and solution pH. Parallelisation allows for high-throughput reactivity screening, increasing the potential for discovery while minimising time constraints, to allow for rapid feedback. Additional modulation of reactivity can then be provided by stirring or heating with discoveries in the search space identified by crystallisation. The automation of these fundamental synthetic processes, controlled by digital code and combined with the plug-and-play aspect the platform functionality, is designed to provide the MWP with wide-ranging utility.

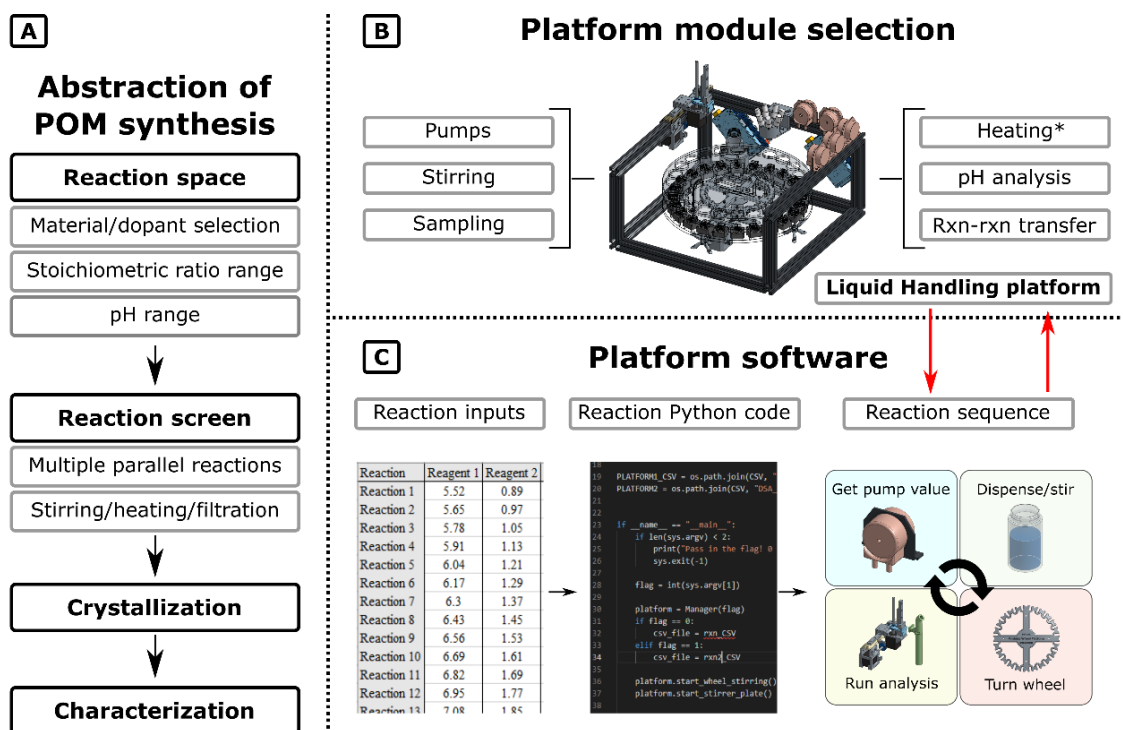


Fig. 1 A) Abstraction of Inorganic/Polyoxometalate synthesis. **B)** The MWP is built using modules selected by the user to perform the required operation (*Heating performed using an auxiliary module, check SI section 1.2). **C)** Reaction inputs via CSV/JSON files are communication to the hardware from an executable synthesis code, all handled by our in-house software.

The base unit of the MWP, capable of running 24 parallel reactions, can be assembled in 5-6 hours (Fig. 2). A Geneva wheel mechanism allows the platform to dispense 24 sequential reaction mixtures via high-accuracy peristaltic pumps with each reactor individually stirred by a custom magnetic stirring module. A series of compact and standalone modules capable of x, y, z movement along the platform frame have been developed allowing for in-line measurement of probe-based feedback, sample extraction for analysis and transfer between vials. Standalone multi-reaction heating/stirring, and filtration modules were also developed as part of the workflow (see SI section 1.2). All custom hardware is controlled using Arduino Mega2650 via in-house, open-source software designed with the same modular approach in mind.

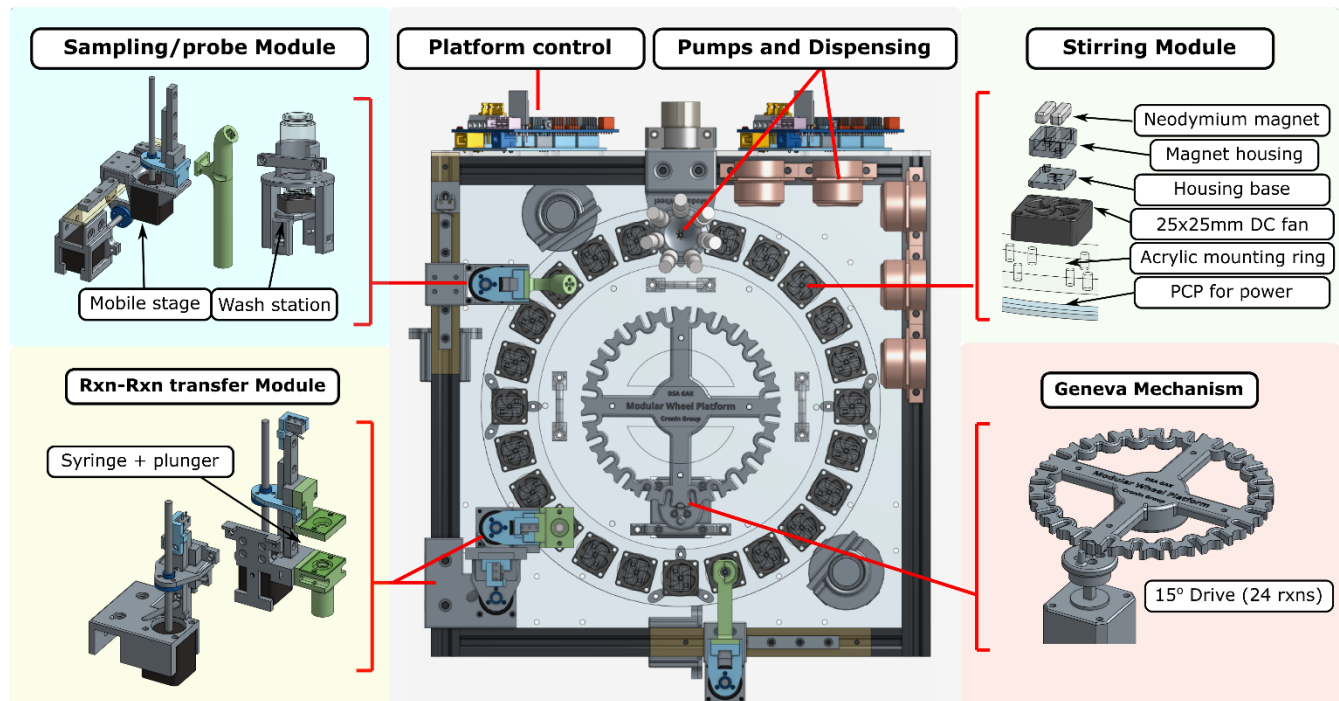


Fig 2. Top view of a Modular wheel platform equipped with numerous modules and accompanying functions. Detailed descriptions of these individual modules can be found in SI section 1.2.

Digital Code

Converting the synthesis of inorganic clusters into digital code essentially creates an executable series of operations that can be performed on any given hardware workflow that has the appropriate functions (SI

Fig 1.11). In our case this involves converting steps such as dispensing reagents, general stepper motor control, pH recording etc. into an executable digital code for each reaction. As chemical discoveries are made, this digital code becomes far more than a series of mechanical operations, it is then a reproducible means of forming these new discoveries. Ultimately that was the goal of this work, to create digital executable reaction code that can be implemented anywhere to be able to reproduce discoveries (SI Fig. 1.12).

Automated Inorganic Synthesis

The Modular Wheel Platform (MWP) was then employed to undertake the exploration of two different sets of chemical space producing compounds [1-4]: $(C_2H_8N)_{10}Na_2[H_6Fe(O_2)W_{24}O_{82}(H_2O)_{25}]$ (1, $\{W_{24}Fe\}$), $(C_2H_8N)_{72}Na_{16}[H_{16}Co_8W_{200}O_{660}(H_2O)_{40}] \cdot 600H_2O$ (2, $\{W_{200}Co_8\}$), $(C_2H_8N)_{72}Na_{16}[H_{16}Ni_8W_{200}O_{660} \cdot (H_2O)_{40}] \cdot 360H_2O$ (3, $\{W_{200}Ni_8\}$) and $(C_2H_8N)_{14}[H_{26}W_{34}V_4O_{130}] \cdot H_2O_{32}$ (4, $\{W_{34}V_4\}$), along with many other known species, for example simple Keggin clusters and 1D $\{W_{11}M^{2+}\}$ chains.

Space 1, consisted of 60 reactions, all with constant volumes of aqueous stocks solutions of sodium tungstate (Na_2WO_4 , 0.723 M, 5 mL), dimethylamine hydrochloride (DMA.HCl, 2.43 M, 4 mL), hydrochloric acid (HCl, 0.5 M, 0.1 mL) and sodium dithionite ($Na_2S_2O_4$, 0.5 M, 0.73 mL) whilst varying the contributions of four transition metal solutions of Fe^{2+} , Co^{2+} , Ni^{2+} and Mn^{2+} (0.5 M, 0.0875-0.425 mL). All reactions performed on this MWP total between 10-13 mL in volume, which has the advantage of economical reagent use whilst also minimizing product crystallization periods. In order to systematically investigate the reaction system generated by these four MCl_2 stock solutions, we considered the parameter space in three dimensions containing all the possible compositions and combinations. The six edges of this tetrahedral space give binary combinations (M_1/M_2), the four faces tertiary combinations ($M_1/M_2/M_3$), and the inner volume quaternary combinations ($M_1/M_2/M_3/M_4$). This approach allowed us to generate a two-dimensional array in the following combinations: Co^{2+}/Ni^{2+} ,

Mn^{2+}/Co^{2+} , Ni^{2+}/Fe^{2+} , Fe^{2+}/Mn^{2+} and $Co^{2+}/Ni^{2+}/Mn^{2+}/Fe^{2+}$. Both representations of Space 1 and the MWP itself are shown in Fig. 3.

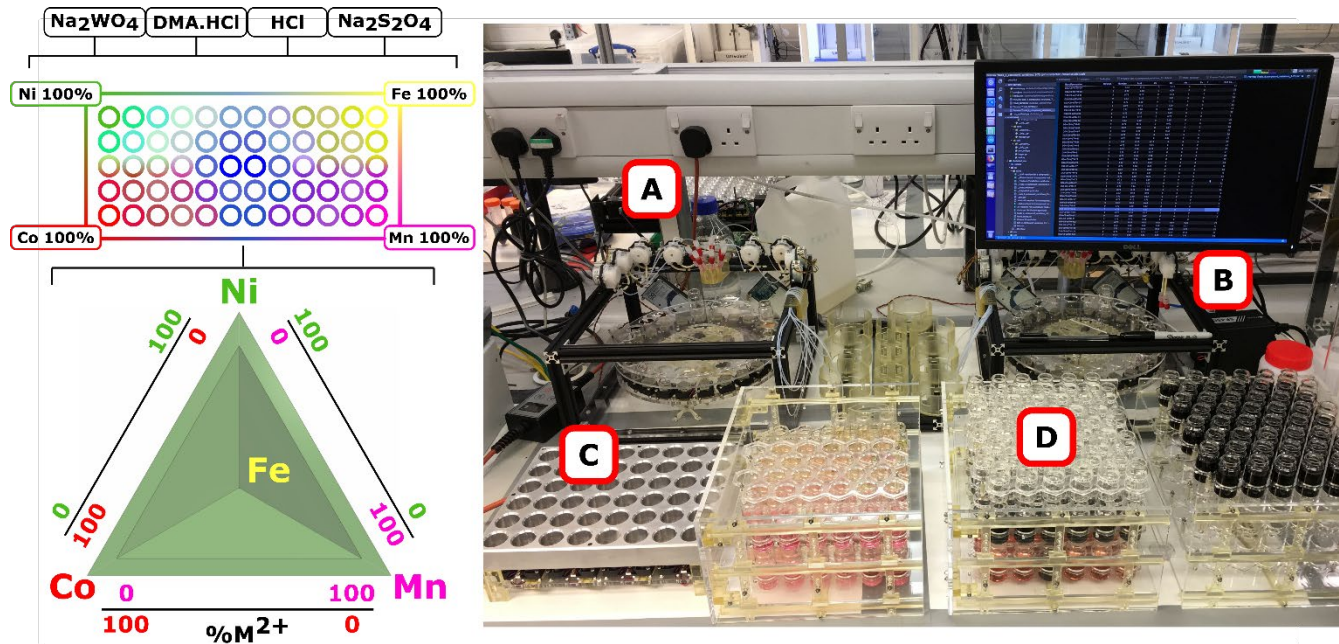


Fig. 3. Space 1 2D and 3D representations (Top left and bottom left respectively). Modular wheel platform (A), PC and platform power supply (B), accompanying heating stirring mantle (C), Reaction samples storage for crystallization (D).

Space 1 resulted in a range of unique formations represented by complexes [1-3], ranging from simple Keggin structures to gigantic $\{W_{200}M_8\}$ clusters. The most significant discovery of this space to date has been the formation complex [1] containing a stable Fe^{3+} -O-O superoxide moiety, bridging two $\{W_{11}\}$ fragments (Fig. 4). The cluster forms as large growths of overlaying light-yellow cuboid crystals (SI Section 2.5 image A, Fig. 2.6 image G) at between pH 2.50 - 3.15. The highest yield to date of this reaction has been 192 mg (10.59 % based on W). When attempting to optimize/repeat this reaction it was found that compared to other examples in this work, this reaction is relatively insensitive to pH but highly sensitive to $FeCl_2$ and reducing agent stoichiometry, slight deviation of their relative ratios failed to produce this cluster. In fact, upon purchasing fresh batches of $Na_2S_2O_4$ and $FeCl_2 \cdot 4H_2O$, lowering both of their relative ratios was required to achieve continued reproducibility demonstrating the sensitivity of

these conditions to reagent purity (SI Section 2.1.5). An μ_{eff} of 5.83 μB for the Fe centre, determined by Evans method ^1H NMR, reveals a high spin d^5 state indicative of a Fe^{3+} centre (see SI 2.4). Thus oxidation of the original Fe^{2+} source under reducing conditions, combined with an O-O bond length of 1.245 Å and the characteristic signal bands of νOO at 967 cm^{-1} by Raman and 1013 cm^{-1} by IR, confirms the formation of a superoxide¹⁷⁻¹⁸ presumably from atmospheric oxygen. The mechanism of this change is likely similar to the binding of oxygen in haemoglobin.¹⁹ Superoxide formation on a POM has been proposed as an intermediate step of an O_2 activation process in $[\text{Ru}^{3+}(\text{OH})_2(\text{H}_2\text{O})_2\text{SiW}_{10}\text{O}_{36}]^{4-}$ by Kuznetsov *et al*²⁰ and a single example of a POM enhancing the oxidative power of a mixed zero-valent iron nanoparticle/ferrous ion solution in the presence of O_2 has been reported.²¹ However, to the best of our knowledge this cluster is a unique example of an end-on (η^1) Fe-superoxide embedded in a tungsten oxide framework, formed under mild conditions and stable for months in the solid state.

Also discovered in Space 1 were samples of $\{\text{W}_{200}\text{M}_8\}$ containing Co^{2+} and Ni^{2+} , forming in numerous reactions at rather unexpected positions in the space. We have previously reported the isolation of $\{\text{W}_{200}\text{Co}_8\}$ however this robotic discovery represents the first time the nickel analogue has been observed.²² This structure requires between 4-10 weeks of crystallization time and the products are typically produced in very low yield meaning many samples containing these compounds can become contaminated with crystals of starting materials or alternative higher-yielding products. This phenomenon ranged from samples containing barely 10 crystals with up to three other products present, to vials containing $\{\text{W}_{200}\text{M}_8\}$ as the sole product in relatively high yield given its rarity and size. One fortunate attribute of this compound is that well-formed crystals of the cluster have a highly distinctive serrated star shape (see SI 2.5), making initial indication of its presence over time easier to observe. In this space 14 of the 60 reactions produced $\{\text{W}_{200}\text{M}_8\}$ ($\text{M} = \text{Co}$ or Ni) in varying purity and yield, with [2] ($\text{M} = \text{Co}$) representing the majority of these samples.

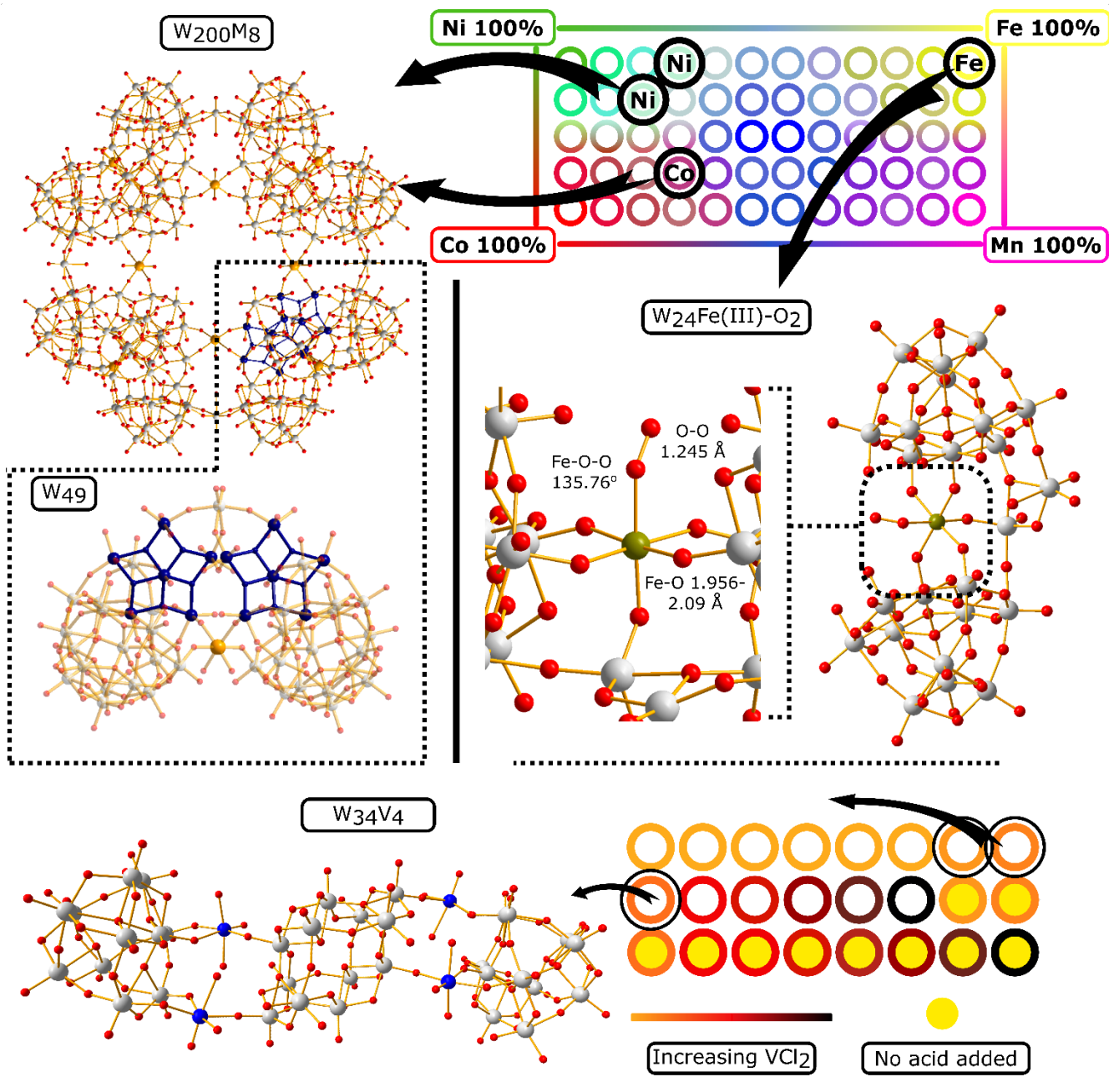


Fig. 4. Mixed W/M space search and compound discovery locations (Top right). $\text{W}_{200}\text{M}_8/\text{W}_{49}\text{M}$ [2][3] structures (top-left). W_{24}Fe [1] superoxide cluster and detailed view of Fe^{3+} -superoxide centre (middle/right). W_{34}V_4 [4] structure and reaction space (bottom).

For each compound, samples producing the highest yield and purity were selected for analysis. The most successful reaction conditions for the formation of the Co containing cluster $\{\text{W}_{200}\text{Co}_8\}$ [2] was at the specific $[\text{Co}^{2+}]:[\text{Ni}^{2+}]:[\text{Mn}^{2+}]:[\text{Fe}^{2+}]$ ratio of 49.3 : 10.9 : 34.3 : 5.5 at an initial pH of 2.2. This reaction produced a yield of 87 mg (4.1% based on W) with the $\{\text{W}_{200}\text{Co}_8\}$ crystals being the sole formation, a

rare occurrence. The crystal structure of compound [2] revealed the $\{W_{200}\}$ nanosized framework constructed by tungsten-based $\{W_{49}M\}$ building blocks. For $\{W_{200}Ni_8\}$ [3] the binary combination of $[Ni^{2+}]:[Fe^{2+}]$ at 79.5: 20.5 produced the best results. Marginally different in crystal appearance to the pale red/orange of compound [2], these yellow crystals begin as pentagonal plate like growths, one face being concave with a star pattern radiating from the centre, the other being a convex bowl-like shape. Over a period of two months some of these crystals grew out from the pentagonal edges, into a distorted star shape with the same serrated edges as seen in the Co example (see SI section 2.5 for crystal images). The highest yield of this compound was very low (17mg, 0.8% based on W) but sufficient for analysis. Intriguingly, we have not yet been able to isolate either compound [1] or [2] from solutions containing only a single hetero-metal ion in solution.

Continuing from the initial success of Space 1; Space 2 was identical in the contribution of tungstate, reducing agent and DMA, whilst exploring the influence of pH and introducing V^{2+} as the hetero-transition metal ion. The space consisted of 24 reactions and produced $\{W_{34}V^{4+}4\}$ [4] (Fig. 4 bottom). The characteristic initial blue colour faded over a period of 2 hours at RT and the remaining brown/black, opaque mixtures filtered simultaneously using the filtration array (see SI Section 1.2.7). Black needle-shaped crystals formed in low/moderate yield within two weeks in 3 of the 24 samples as the initial pH proceeded toward 2.20. The highest yielding sample produced just 21 mg (1.12% based on W) of pure product. This yield is mainly due to the difficulty in isolation of the small needles from other crystallized products (mainly Na_2WO_4). The significant pH difference from the reactions in Space 1 was due mainly to the presence of VCl_2 . Increasing the stoichiometry of VCl_2 further resulted in pH values < 2.0 and little or no formation of the compound was observed. This shows a narrow window of pH in which [4] is produced at between 2.20-2.75. The structure forms a §-shape between three distinct fragments, two terminal $\{W_{11}\}$ and a central $\{W_{12}\}$ cage via VO_6 linkages. The V^{2+} source undergoes expected oxidation

in air to produce V⁴⁺ with both terminal V=O and bridging V-O-W bonds, shown clearly in the crystallographic data. All bridging VO₆ therefore have distorted octahedral geometry allowing for the unequal arrangement of bonding between the central and terminal fragments, the central cage being bound to the V centres via a single η² V-O-W bond and the terminal {W₁₁} fragments bound by two η³ V-[O-W]₂ bridges.

Compounds [1] and [4] are similar to the {W₂₂} and {W₃₄} iso-polyoxotungstate species published by our group in 2008 with the W-O-W linkages between distinct W-subunits being replaced fully or in part by heterometal-oxo linkages.²³ For [1] the two {W₁₁} subunits are essentially mirror images of one another across two bridging tungsten atoms and central Fe atom forming a flexible cavity for the Fe position as opposed to the S-shape made by the same subunits in this previous paper. Compound [4] however is remarkably similar to the {W₃₄} iso-polyoxotungstate. In that paper we theorized that the lacunary positions on the {W₁₁} subunits present in these compounds could offer opportunities to further increase the structural diversity of this class of molecules and the work described herein is the first example, to our knowledge, of the realization of that hypothesis.

Conclusions

We have created a high-throughput, inexpensive modular platform for the exploration of inorganic synthesis space and have utilized this device in the discovery of new metal oxide clusters. These discoveries, made between narrow windows in the chemical space, could easily have been missed or proved irreproducible during bench synthesis. Most notable is the discovery of the first stable POM-superoxide species within such a heavily explored chemical space. The fact that mixed transition metal W-based POM synthesis has been studied for decades and yet the simple synthesis of this novel structure remained unobserved until now shows the utility of this robotic system. The medium scale batch

approach of systematic chemical space exploration allowed for the reproducible synthesis and crystallization of these systems while the platform's accuracy and efficiency allowed for extensive exploration of the chemistry selected for investigation; as well as mapping of the fine boundaries between crystal formation and failure with minimal effort. In the near future we intend to add greater functionality to this modular architecture, advancing its liquid handling capabilities and incorporating multiple sensor types. Our immediate intention is to integrate spectroscopic capabilities, centred around the modular wheel platform, that can provide direct reaction feedback to create closed-loop systems working autonomously. With this direct access to reaction feedback, we hope to incorporate the use of algorithms in the decision-making process for future reaction conditions, a method that have shown such promise in other reported work.²⁴⁻²⁵

Experimental Section

Full details of the platform hardware and software can be found in the SI – Section 1 and ask Lee Cronin for the repo before peer reviewed publication.

Synthesis of compounds [1-4] proceeded by the following sequence: Aqueous stock solutions were dispensed in the following order: 1. Sodium tungstate [0.66 M adjusted to pH 3 using conc. HCl]; 2. Dimethylamine hydrochloride ($\text{CH}_3)_2\text{NH}\cdot\text{HCl}$ [2.453 M]; 3. Hydrochloric acid [0.5 M]; 4. Sodium Dithionite $\text{Na}_2\text{S}_2\text{O}_4$ [0.5 M]; 5. Up to four transition metal solutions [0.5 M]. Full reactions grids can be found in SI Section 2. Reactions were stirred at ca. 800 rpm for 1-2 h in a 14 mL disposable glass vial and vacuum filtered using the filtration array through PTFE frits/filter paper. Crystallization times varied from 1 week to 2 months (see SI). **Compound [1]** $\text{Na}_2(\text{C}_2\text{H}_8\text{N})_{10}[\text{H}_6\text{W}_{24}\text{Fe}(\text{O}_2)\text{O}_{82}]\cdot 20\text{H}_2\text{O}$: $\text{C}_{20}\text{H}_{126}\text{FeN}_{10}\text{Na}_2\text{O}_{104}\text{W}_{24}$; Average yield across 5 repeat reactions: 0.104 g (9% based on W); yellow block crystals; Triclinic; space group $P-1$, $M_r = 6685.53 \text{ g}\cdot\text{mol}^{-1}$, $a = 13.1545(16)$, $b = 18.807(2)$, $c = 25.522(3) \text{ \AA}$, $\alpha = 104.421(2)$, $\beta = 104.482(2)$, $\gamma = 96.678(2)^\circ$; $V = 5812.3(12) \text{ \AA}^3$, $Z = 2$; $\rho = 3.820 \text{ Mg}\cdot\text{m}^{-3}$

³, λ (Mo-K α) = 0.71073 Å, 197690 Reflections measured, 22842 unique reflections [$R_{(int)}$ = 0.0365] which were used in all calculations, 1379 refined parameters, final RI = 0.0300 and $wR2$ = 0.0711 (all data); Raman O-O superoxide peak 967 cm⁻¹ (s); Elemental analysis Calculated (%) W(65.88), Fe(0.87), C(3.59), H(1.9), N(2.11) Found (%) W(65.58), Fe(0.92), C(4.06), H(1.81), N(2.28). **Compound [2]** reproduced as previous work (CSD 895471). **Compound [3]** Na₁₆(C₂H₈N)₇₂[H₁₆W₂₀₀Ni₈O₆₆₀(H₂O)₄₀].450H₂O: C₁₄₄H₁₅₇₂Ni₈N₇₂Na₁₆O₁₁₅₀W₂₀₀, M_r = 60330.16 g·mol⁻¹; Yellow serrated star shaped crystals (see SI section 2.5 Crystal images). Tetragonal; space group P42/nmc, a = 48.8657(4), c = 29.4123(2) Å; V = 70232.4(7) Å³; Z = 2; ρ = 2.786 Mg·m⁻³; λ (Mo-K α = 0.71073 Å. 383669 reflections measured; 33492 unique reflections [$R_{(int)}$ = 0.0711] which were used in all calculations; 1132 refined parameters; final RI = 0.0677 and $wR2$ = 0.195 (all data); Elemental analysis Calculated (%) W(60.94), Ni(0.778), C(2.86), H(2.62), N(1.67) Found (%) W(63.02), Ni(0.765), C(3.3), H(1.45), N(1.63). Average yield across 5 repeat reactions 9 mg (0.45 % based on W). **Compound [4]** (C₂H₈N)₁₄[H₂₆W₃₄V₄O₁₃₀]·30H₂O: C₂₈H₂₀₂V₄N₁₄O₁₆₄W₃₄, M_r = 9782.68 g·mol⁻¹; Black needle crystals. Triclinic; space group P-1, a = 13.5219(16), b = 18.592(2), c = 20.285(2) Å, α = 68.689(2), β = 79.219(2), γ = 75.283(2)°; V = 4569.5(9) Å³; Z = 1; ρ = 3.555 Mg·m⁻³; λ (Mo-K α = 0.71073 Å. 57247 Reflections measured; 17941 unique reflections [$R_{(int)}$ = 0.0516] which were used in all calculations; 976 refined parameters; final RI = 0.0421 and $wR2$ = 0.1197 (all data). Elemental analysis Calculated (%) W(62.18), V(2.03), C(3.52), H(1.75), N(2.05) Found (%) W(61.67), V(2.114), C(3.91), H(1.4), N(2.14). Average yield across 5 repeat reactions 14 mg (0.74 % based on W).

Further experimental procedures and compound characterization can be in SI – Section 2.

Author Contributions

LC devised the overall concept and the platform concept and hardware design was by DS, the software architecture and implementation was GK. The chemistry and chemical analysis performed by DS and

Vasilis Duros with help from James McIver and Nicola Bell. The x-ray crystallography was performed by DS and structure elucidation by DL. The chemistry itself was suggested by LC who oversaw the entire project and co-wrote the paper with DS with help from NB. Both DS and GK were directly supervised by Dr Abhishek Sharma as our internal team leader.

Funding Sources

We gratefully acknowledge financial support from the EPSRC (Grant Nos EP/L023652/1, EP/H024107/1, EP/I033459/1, EP/J00135X/1, EP/J015156/1, EP/K021966/1, EP/K023004/1, EP/K038885/1, EP/L015668/1, EP/S030603/1), and the ERC (project 670467 SMART-POM).

References

- (1) Malakoutikhah, M.; Peyralans, J. J. P.; Colomb-Delsuc, M.; Fanlo-Virgos, H.; Stuart, M. C. A.; Otto, S., Uncovering the Selection Criteria for the Emergence of Multi-Building-Block Replicators from Dynamic Combinatorial Libraries. *J. Am. Chem. Soc.* **2013**, *135* (49), 18406-18417.
- (2) Moghaddam, M. M.; Baghbanzadeh, M.; Sadeghpour, A.; Glatter, O.; Kappe, C. O., Continuous-Flow Synthesis of CdSe Quantum Dots: A Size-Tunable and Scalable Approach. *Chem. - Eur. J.* **2013**, *19* (35), 11629-11636.
- (3) Richmond, C. J.; Miras, H. N.; de la Oliva, A. R.; Zang, H. Y.; Sans, V.; Paramonov, L.; Makatsoris, C.; Inglis, R.; Brechin, E. K.; Long, D. L.; Cronin, L., A flow-system array for the discovery and scale up of inorganic clusters. *Nat. Chem.* **2012**, *4* (12), 1038-1044.
- (4) Rubio-Martinez, M.; Batten, M. P.; Polyzos, A.; Carey, K. C.; Mardel, J. I.; Lim, K. S.; Hill, M. R., Versatile, High Quality and Scalable Continuous Flow Production of Metal-Organic Frameworks. *Sci. Rep.* **2014**, *4*, 5443.
- (5) Vila-Nadal, L.; Cronin, L., Design and synthesis of polyoxometalate-framework materials from cluster precursors. *Nat. Rev. Mater.* **2017**, *2* (10) 17054.
- (6) Yoshida, J.; Takahashi, Y.; Nagaki, A., Flash chemistry: flow chemistry that cannot be done in batch. *Chem. Commun.* **2013**, *49* (85), 9896-9904.

- (7) Parrott, A. J.; Bourne, R. A.; Akien, G. R.; Irvine, D. J.; Poliakoff, M., Self-Optimizing Continuous Reactions in Supercritical Carbon Dioxide. *Angew. Chem. Int. Ed.* **2011**, *50* (16), 3788-3792.
- (8) Vila-Nadal, L.; Rodriguez-Forte, A.; Yan, L. K.; Wilson, E. F.; Cronin, L.; Poblet, J. M., Nucleation Mechanisms of Molecular Oxides: A Study of the Assembly-Dissassembly of $[W_6O_{19}]^{(2-)}$ by Theory and Mass Spectrometry. *Angew. Chem. Int. Ed.* **2009**, *48* (30), 5452-5456.
- (9) Miras, H. N.; Yan, J.; Long, D. L.; Cronin, L., Engineering polyoxometalates with emergent properties. *Chem. Soc. Rev.* **2012**, *41* (22), 7403-7430.
- (10) Rhule, J. T.; Hill, C. L.; Judd, D. A., Polyoxometalates in medicine. *Chem. Rev.* **1998**, *98* (1), 327-357.
- (11) Wang, S. S.; Yang, G. Y., Recent Advances in Polyoxometalate-Catalyzed Reactions. *Chem. Rev.* **2015**, *115* (11), 4893-4962.
- (12) Wang, S. M.; Hwang, J.; Kim, E., Polyoxometalates as promising materials for electrochromic devices. *J. Mater. Chem. C.* **2019**, *7* (26), 7828-7850.
- (13) Chen, J. J.; Symes, M. D.; Cronin, L., Highly reduced and protonated aqueous solutions of $[P_2W_{18}O_{62}]^{(6-)}$ for on-demand hydrogen generation and energy storage. *Nat. Chem.* **2018**, *10* (10), 1042-1047.
- (14) Zang, H. Y.; de la Oliva, A. R.; Miras, H. N.; Long, D. L.; McBurney, R. T.; Cronin, L., Discovery of gigantic molecular nanostructures using a flow reaction array as a search engine. *Nat. Commun.* **2014**, *5*, 3715.
- (15) Smith, R. D. L.; Prevot, M. S.; Fagan, R. D.; Trudel, S.; Berlinguette, C. P., Water Oxidation Catalysis: Electrocatalytic Response to Metal Stoichiometry in Amorphous Metal Oxide Films Containing Iron, Cobalt, and Nickel. *J. Am. Chem. Soc.* **2013**, *135* (31), 11580-11586.
- (16) Duros, V.; Grizou, J.; Xuan, W. M.; Hosni, Z.; Long, D. L.; Miras, H. N.; Cronin, L., Human versus Robots in the Discovery and Crystallization of Gigantic Polyoxometalates. *Angew. Chem. Int. Ed.* **2017**, *56* (36), 10815-10820.
- (17) Cramer, C. J.; Tolman, W. B.; Theopold, K. H.; Rheingold, A. L., Variable character of O-O and M-O bonding in side-on (η^2) 1 : 1 metal complexes of O_2 . *Proc. Nat. Acad. Sci.* **2003**, *100* (7), 3635-3640.
- (18) Fukuzumi, S.; Lee, Y. M.; Nam, W., Structure and reactivity of the first-row d-block metal-superoxo complexes. *Dalton Trans.* **2019** *48*, 9469-9489.
- (19) Paoli, M.; Liddington, R.; Tame, J.; Wilkinson, A.; Dodson, G., Crystal structure of T state haemoglobin with oxygen bound at all four haems. *J. Mol. Biol.* **1996**, *256* (4), 775-792.

- (20) Kuznetsov, A. E.; Geletii, Y. V.; Hill, C. L.; Morokuma, K.; Musaev, D. G., Dioxygen and Water Activation Processes on Multi-Ru-Substituted Polyoxometalates: Comparison with the "Blue-Dimer" Water Oxidation Catalyst. *J. Am. Chem. Soc.* **2009**, *131* (19), 6844-6854.
- (21) Lee, C.; Keenan, C. R.; Sedlak, D. L., Polyoxometalate-enhanced oxidation of organic compounds by nanoparticulate zero-valent iron and ferrous ion in the presence of oxygen. *Environ. Sci. Technol.* **2008**, *42* (13), 4921-4926.
- (22) de la Oliva, A. R.; Sans, V.; Miras, H. N.; Yan, J.; Zang, H.; Richmond, C. J.; Long, D.-L.; Cronin, L., Assembly of a Gigantic Polyoxometalate Cluster {W₂₀₀Co₈O₆₆₀} in a Networked Reactor System. *Angew. Chem. Int. Ed.* **2012**, *51* (51), 12759-12762.
- (23) Miras, H. N.; Yan, J.; Long, D. L.; Cronin, L., Structural Evolution of "S"-Shaped [H₄W₂₂O₇₄]⁽¹²⁻⁾ and "S"-Shaped [H₁₀W₃₄O₁₁₆]⁽¹⁸⁻⁾ Isopolyoxotungstate Clusters. *Angew. Chem. Int. Ed.* **2008**, *47* (44), 8420-8423.
- (24) Granda, J. M.; Donina, L.; Dragone, V.; Long, D. L.; Cronin, L., Controlling an organic synthesis robot with machine learning to search for new reactivity. *Nature* **2018**, *559* (7714), 377-381.
- (25) Raccuglia, P.; Elbert, K. C.; Adler, P. D. F.; Falk, C.; Wenny, M. B.; Mollo, A.; Zeller, M.; Friedler, S. A.; Schrier, J.; Norquist, A. J., Machine-learning-assisted materials discovery using failed experiments. *Nature* **2016**, *533* (7601), 73-76.

Supporting information for:

A Modular Programmable Inorganic Cluster Discovery Robot for the
Discovery and Synthesis of Polyoxometalates

Daniel S. Salley, Graham A. Keenan, De-Liang Long, Nicola Bell, Leroy Cronin*

School of Chemistry, The University of Glasgow, Glasgow, G12 8QQ, UK. †These authors contributed equally to this work.

*Correspondence to: Lee.Cronin@glasgow.ac.uk; <http://www.croninlab.com>

Contents

1.	Robotic platform and concept:	2
1.1	Overview.....	2
1.2	Modules.....	2
1.2.1	Base platform- Geneva wheel mechanism.....	2
1.2.2	Stirring assembly.....	3
1.2.3	Pump, dispensing and control	3
1.2.4	X, Y, Z movement for analysis	4
1.2.5	Dual syringe driver for reaction-reaction transfer.....	5
1.2.6	Heating/stirring	6
1.2.7	Filtration.....	7
1.3	Software	9
1.3.1	General overview	9
1.3.2	Core layer.....	9
1.3.3	Experimental layer	10
1.3.4	Analytical layer.....	10
1.3.5	Digital code	11
2.	Experimental	13
2.1	Reaction conditions and chemical Space 1 and 2	13
2.1.1	Space 1 stock solutions and reactions:	13
2.1.2	Space 2 stock solutions and reactions	15
2.1.3	Reaction details.....	16
2.1.4	$(C_2H_8N)_{10}Na_2[H_6Fe(O_2)W_{24}O_{82}(H_2O)_{25}]$ (1, {W ₂₄ Fe}) – Initial Discovery	16
2.1.5	$(C_2H_8N)_{10}Na_2[H_6Fe(O_2)W_{24}O_{82}(H_2O)_{25}]$ (1, {W ₂₄ Fe}) – Reproduction, fresh reagents	16
2.1.6	$(C_2H_8N)_{72}Na_{16}[H_{16}Co_8W_{200}O_{660}(H_2O)_{40}] \cdot 600H_2O$ (2, {W ₂₀₀ Co ₈ }),.....	17
2.1.7	$(C_2H_8N)_{72}Na_{16}[H_{16}Ni_8W_{200}O_{660}-(H_2O)_{40}] \cdot 360H_2O$ (3, {W ₂₀₀ Ni ₈ })	17
2.1.8	$(C_2H_8N)_{14}[H_{26}W_{34}V_4O_{130}] \cdot (H_2O)_{32}$ (4, {W ₃₄ V ₄ }),.....	18
2.2	Crystallography and crystal data.....	18
2.3	Compound [1] IR and Raman data	23
2.4	Compound [1] Evans Method NMR and U _{eff}	24
2.5	Crystal images.....	25

1. Robotic platform and concept:

1.1 Overview

Control of this platform is not computationally expensive and so any recent standard desktop or laptop computer is sufficient. This project employed a Lenovo ThinkCentre running Linux Ubuntu. All stepper motors, pumps, end stop switches and fans were controlled via an Arduino Mega 2560/RAMPs combination via our in-house software. Pumps are calibrated to 2 decimal places before all reaction series (recalibrated every 120 reactions if the series is longer). Tubing used is either PTFE for transport between stock-pump and pump-vial or Novoprene[®] for within the peristaltic pumps. All 3D printer components were printed using an Objet500 Connex printer. All links, STL files, software and instruction for the construction and operation of the platform used in the course of this work can be found in the GitHub links to follow.

1.2 Modules

1.2.1 Base platform- Geneva wheel mechanism

The base platform of the robot is composed of a frame of v-slot aluminium rails with an acrylic cut base plate responsible for guiding the position of the Geneva drive parts and stirring assembly. The mechanism range is from a 4-30 position reaction plate based on the user's needs. For this work a 15°, 24 slot Geneva drive was used (Fig. 1.1). The vial tray is cut from 4/6mm acrylic, the rails made of anodized aluminium, a Nema17 stepper motor turns the drive and all other parts seen are 3D printed.

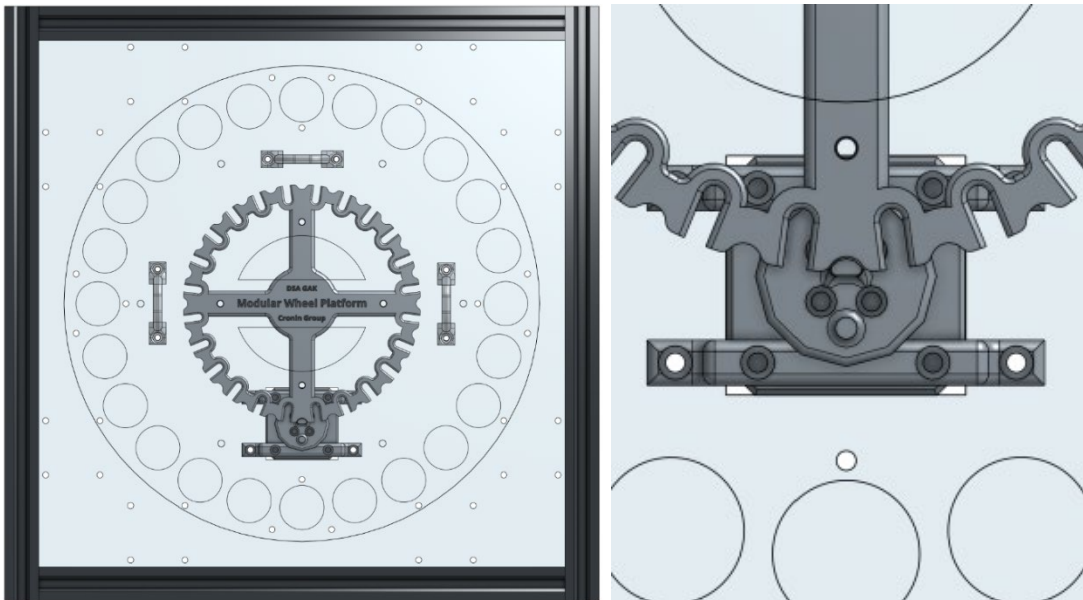


Figure 1.1. Top view of base structure. (Left) Base frame and acrylic plate, 24 reaction vial tray, 3 levelling arcs, Geneva driven wheel mounted on a Nema17 stepper motor and a 15° Geneva drive wheel. (Right) Drive to driven

The platform is powered using a Corsair SF450 modular unit.

1.2.2 Stirring assembly

Most chemistry requires some type of agitation/mixing to function properly, however individual effective stirring can be difficult to achieve with small scale reactions run in parallel. Given most stirring apparatus is expensive and have footprints too large to be sufficient on this platform, a simple and inexpensive solution was created using Arduino controlled 25 x 25 mm DC fans, with a custom 3D printed housing for two rectangular neodymium magnets attached on top. These assemblies are housed on a magnetically mounted acrylic cut ring and powered via an in-house made PCB strip attached to the base of the ring. Using the MOSFET functions on the RAMPs boards, restricted current is supplied to the fans, determined via a PWM setting given by the user to lower the RPM from the standard 9000 of the unhindered fans to 200-1000 RPM. The magnets each have a 2.2 kg pull and when oriented correctly, provide powerful and consistent stirring speeds for 12 mm Teflon coated magnet stir bars used in this work (Fig. 1.2). The same principle has been applied to larger fans with more powerful magnets to achieve stirring in volumes from 50-1000 mL with appropriate stir bars.

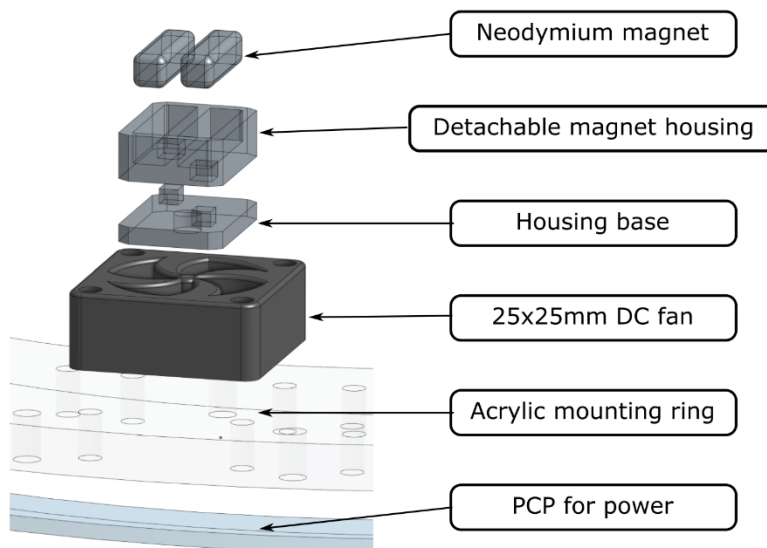


Figure 1.2. Exploded view of custom stirring assembly

1.2.3 Pump, dispensing and control

High accuracy, low expense SR10-30 peristaltic pumps from Thomas by Gardner Denver were used for this work. The pumps are controlled by Arduino Mega 2560 using our in-house software. Our software allows for commands to be sent to any Arduino based device directly from Python streamlining the process of hardware operation. The Arduino uses RAMPs fitted with DRV8825 stepper motor driver boards to control up to 5 stepper motors. There are 3 MOSFET outputs and numerous other electronics per board that can be utilized for various functions. For this work 2 Arduino/RAMPs combinations were needed to control 10 stepper motors (7 for pumps, 1 for the Geneva drive and 2 for the x,y,z movement

module used for measuring pH) and other components detailed later. Up to 21 inputs can be dispensed from any individual position on the wheel via a custom 3D printed housing, for this work 7 were needed. The Arduino/RAMPs are housed on an acrylic cut sheet mounted on the side of the platform (Fig. 1.3). This means moving/transporting the platform is simple as USB and power connectivity are the only exterior wiring required with all other power/control cables being localized to the platform.

Liquid handling involved the following components (links in the GitHub page provided (See Section 1.4), Wheel platform / platform / hardware / build / materials):

- 1/16" OD PTFE tubing
- Flangeless fittings, polypropylene 1/4-28 flat bottom for 1/16" OD
- Restek female to male Luer assay 1/4-28
- Teflon lined dispensing needles

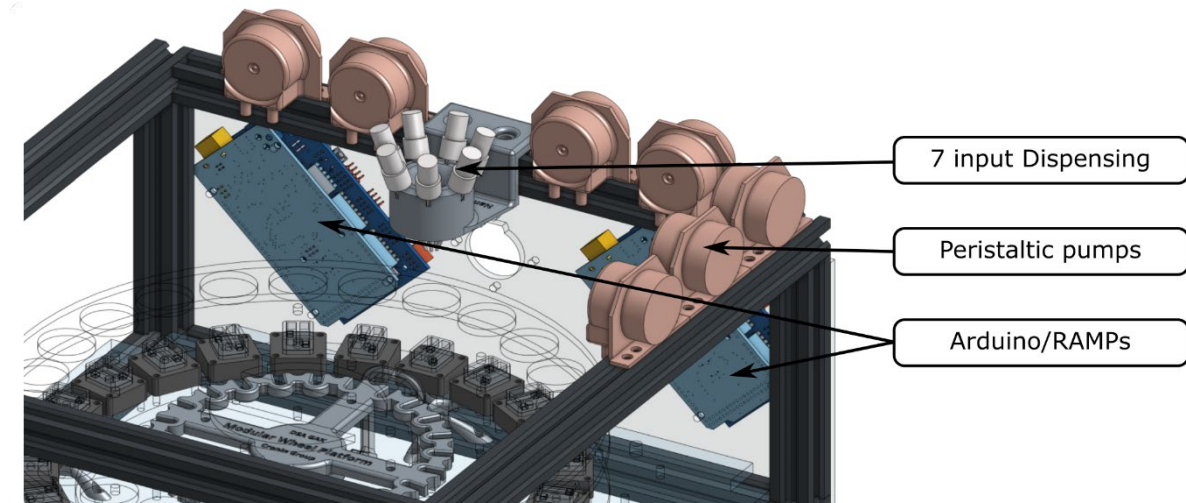


Figure 1.3. Pumps, control boards and dispensing

1.2.4 X, Y, Z movement for analysis

For in-line automated analysis, a number of essential functions were needed to ensure efficiency and eliminate contamination between reactions. First the module required Z direction movement to access the sample and allow the wheel to continue movement, second was a cleaning method for tubes/probe with the ability to reach it and finally it needed to be compact to allow for numerous stations to be installed on a single platform. Standard practice would be to use a linear actuator for these functions however, for our needs a linear actuator would be far too large and intrusive with limited room for multiple functions. A custom modular syringe driver (MSD) was developed with several attachments for a variety of functions. This unit uses a NSK PU series 9 mm linear guide rail and carriage in both the horizontal and vertical movements. The movement is powered by two custom Nema11 stepper motors with threaded columns, powered and controlled as above, with the movement limits defined by

electronic end-stop microswitches. The unit is mounted under the v-slot frame. The unit, displayed in Fig. 1.4, shows the Z-motion motor mounted inside the platform frame, a motor outside the frame version is available from the repository provided and all parts are symmetrical meaning any vial position can be accessed via these modules. Also included in Fig. 1.4 is the stirred wash station apparatus for probes/tubing. These are directly included on the base plate of the platform. The wash solution is removed and replenished after each wash cycle by the same peristaltic pumps used to dispense reagents.

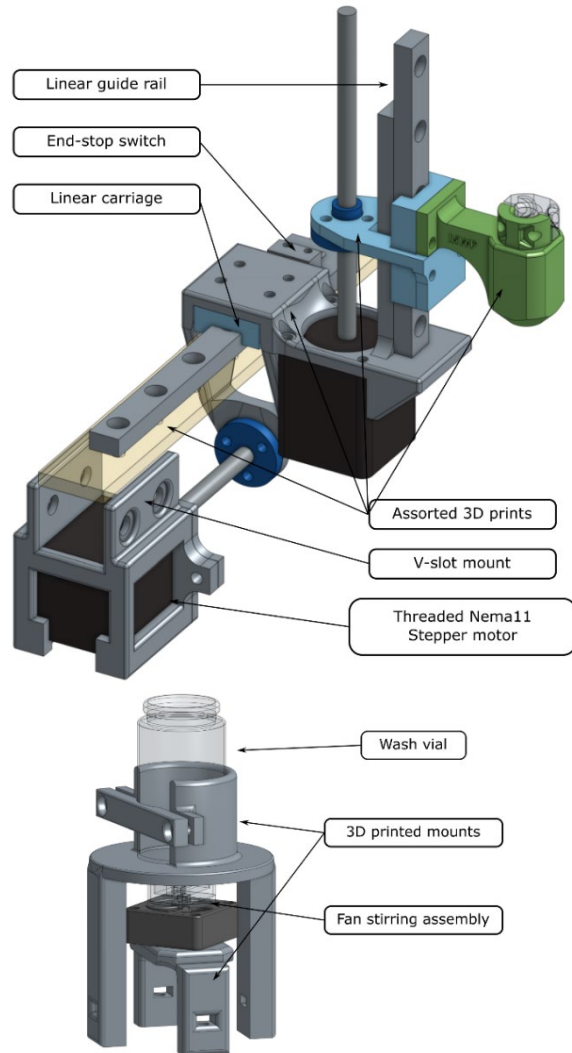


Figure 1.4. Modular syringe driver Z and X/Y movement with probe mount (above).

Magnetically stirred wash station (below) components

1.2.5 Dual syringe driver for reaction-reaction transfer

This module was designed to allow for reaction materials to be transferred between vials for processes like reaction seeding or serial dilution. The module can be fitted with any syringe size up to 25 mL depending on the material being transferred. The unit itself uses two of the same linear guide/carriage and microswitch combinations as before, both travelling in the Z direction. Assembly 1 (Fig. 1.5) holds

a syringe in a static position with the moving carriage accurately controlling the position of the syringe plunger. Assembly 2 (Fig. 1.5) houses the entire syringe assembly in order that it can be moved in and out of the reaction vials. The motor position accuracy is such that microliter volumes can be removed and transferred between reactions. Though not employed in this work, the module is already at work in another project involving the MWP.

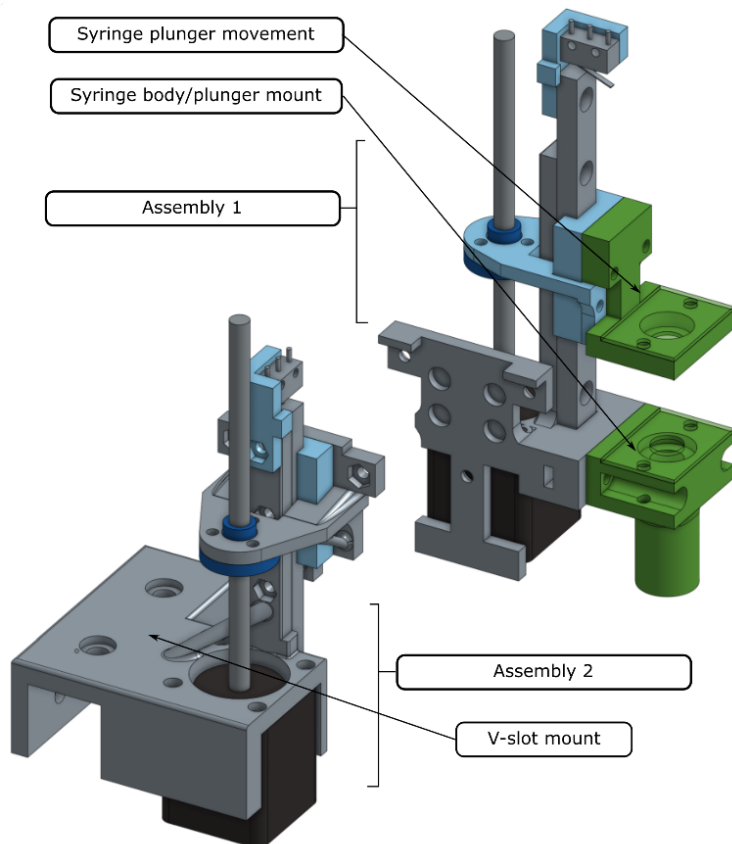


Figure 1.5. Exploded view of dual syringe driver for reaction-reaction transfer

1.2.6 Heating/stirring

The throughput capabilities of the platform and the large chemical space to be explored in this work necessitated a method for long-term reaction heating and stirring. Given the expense and relatively large, footprint to stirring positions of conventional heating/stirring plates, it was necessary to create a module designed for the scale of this platform. The following parts were designed and made in house or ordered from commercially available sources to achieve a stirring and heating mantle for 48 reactions for less than £600 (compared to £3500+ for 12 stirring positions from Ika) (Fig. 1.6):

- A silicone heating plate within line temperature control
- A single 48-well unit milled from aluminium
- An acrylic base plate to house 48 stirring mechanism assemblies detailed above.

- PCP strips mounted on the underside of base plate to power all stirring assemblies.

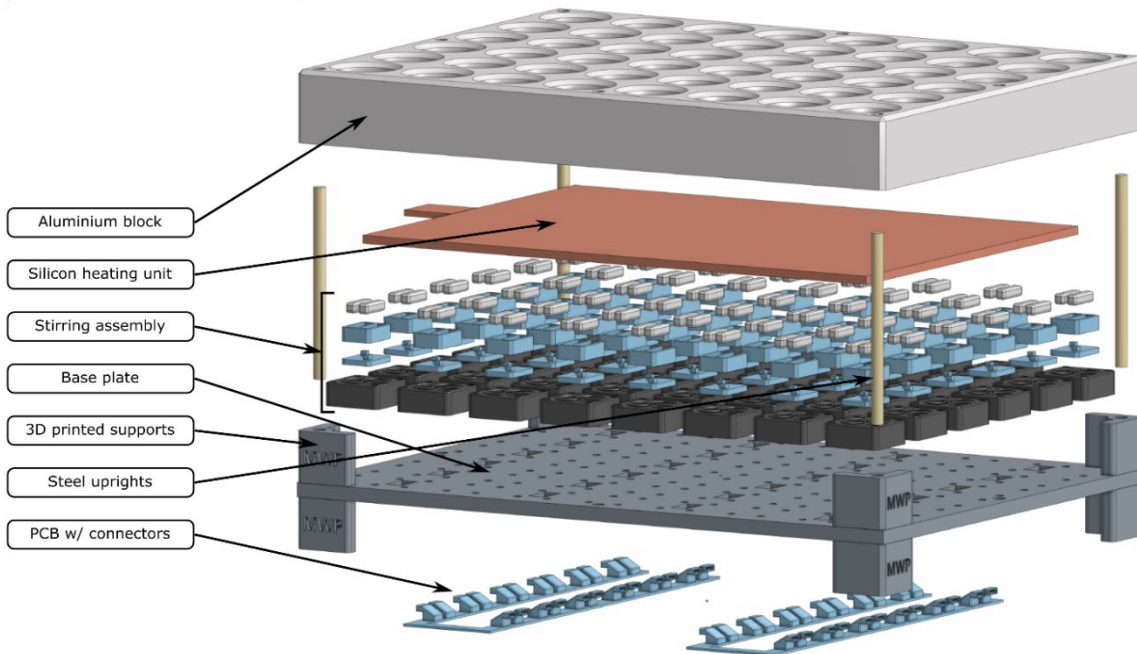


Figure 1.6. Stirring/Heating mantle for 48 reactions (14 mL vials)

1.2.7 Filtration

To handle the high throughput of reactions that form precipitate (the majority of reactions in this work) a similarly capable filtration method was required. The module developed for this purpose is capable of vacuum filtration of 48 reaction solutions through a host of desired materials (in this work silica or standard Whatman filter paper). A construction of fused acrylic and dual material (rigid and rubber) 3D printed components produced an adequately seal to be able to use any standard vacuum pump to achieve filtration. Teos 25 mL fritted columns containing the filtration material served for all reactions in this work. This module saves significant time and ensures clean reaction solutions (Fig. 1.7).

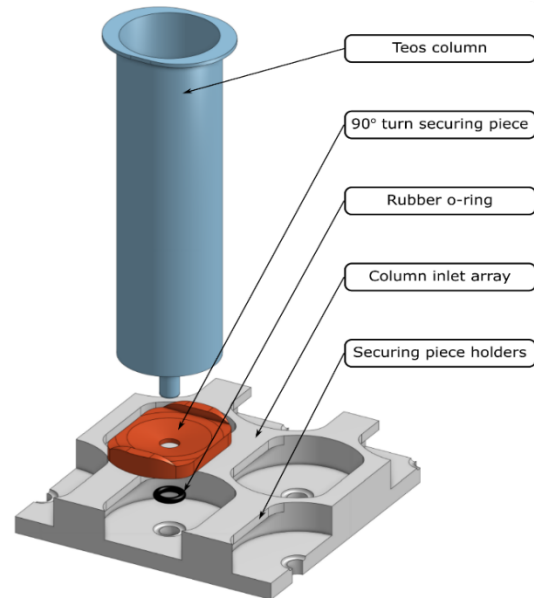
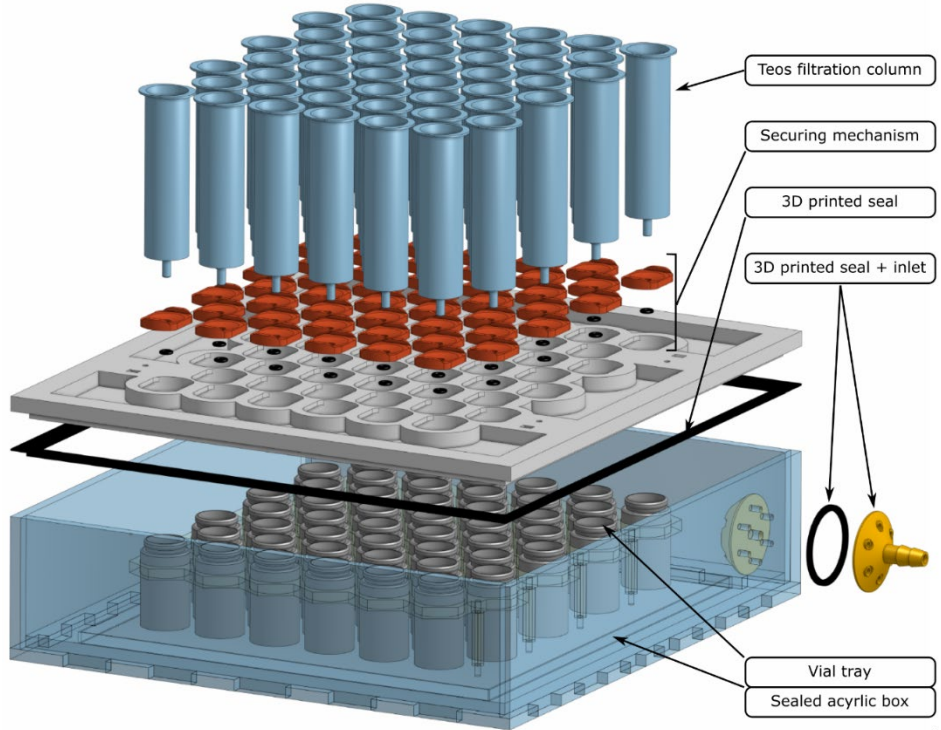


Figure 1.7. Exploded view of filtration mantle (above) Exploded view of individual filtration inlet and securing mechanism

1.3 Software

1.3.1 General overview

The software architecture of these systems is split into three distinct layers – Core, Experimental, and Analytical. The Core layer is the heart of the robotic system; this is where the control software for interacting with the automated hardware is housed. The Experimental layer is where the user defines their code to interface with the Core layer in order to perform experiments. The Analytical layer is used to store code which performs analysis on experimental data produced by the system. This can take many forms from simple analytical techniques to fully implemented machine learning algorithms. However, as these automated systems can be used as just a simple experimental aid without the need for analysis, this Analytical layer is optional.

1.3.2 Core layer

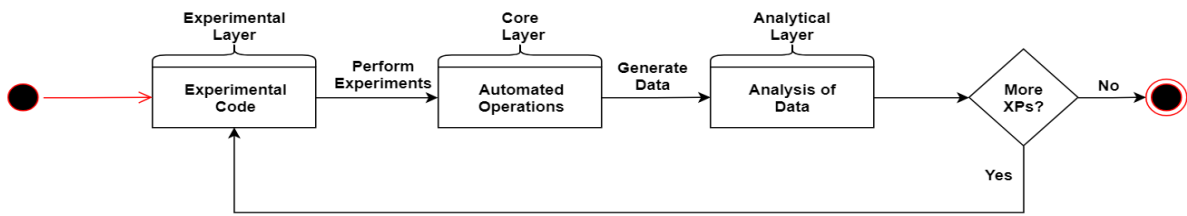


Figure 1.8. Outline of the experimental workflow using the suggested architecture.

The Core layer holds all the software responsible for interfacing with the hardware components of the system. Using the façade design pattern, the user can have a single, high-level interface in which to interact with the underlying hardware of the system. Each hardware component (module) is comprised of two sub-layers, Base and Operational. The Base sub-layer is responsible for the declaration of a base class comprised of low-level methods that perform some basic setup for a piece of hardware. For example, a Spectrometer base class would be responsible for interfacing with attached spectrometers and setting up some basic functionality such as obtaining a measurement or averaging out a series of measurements. The Operational sub-layer is a child class of the Base sub-layer. This is intended for higher level functionality on top of the parent class. Continuing with the Spectrometer example, an Operational Spectrometer child class would consist of methods responsible for obtaining a measurement and saving the raw output and image to file. Once a series of modules have been implemented, they are accessed via a final Managerial sub-layer. The Managerial layer is a single manager class that instantiates all Operational sub-layer classes and provides methods for interfacing between them all (Fig. 1.9). Here is where the user would define methods that would perform operations that require the use of different modules together. An example could be sampling liquid for spectrometric analysis (Pump, Robotic and Spectrometer modules). The Managerial sub-layer here acts as the façade, a single class that the user interacts with in order to complete operations with the system. Utilising this pattern, development of new modules is simple. The user defines a Base and Operational layer for the new module and declares it in the Managerial layer. This modular approach enables the user the choice of

which modules they wish to include/discard and develop new modules if needed in a plug-and-play fashion.

1.3.3 Experimental layer

Core Layer

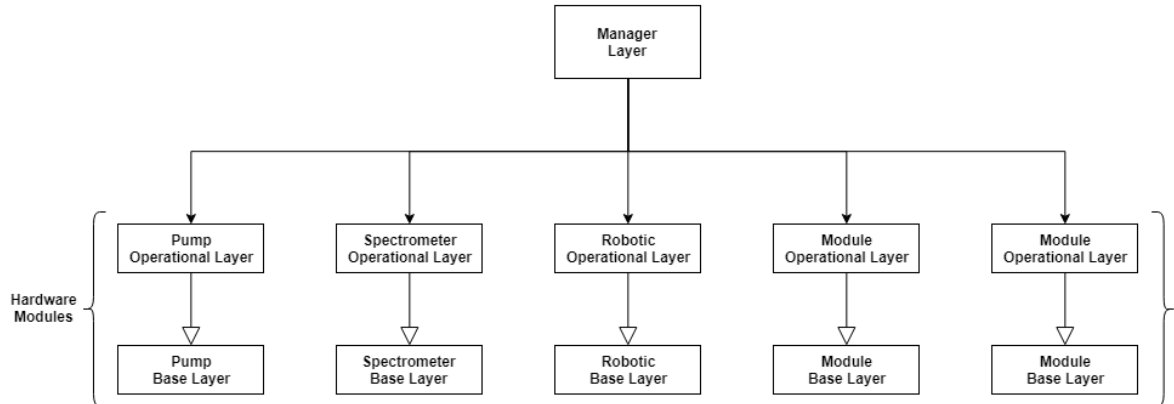


Figure 1.9. UML-like representation of the Core Layer Architecture. Each module has a defined Base and Operational layer component. These are accessed through a single Manager class that defines a series of user-defined methods for accessing each module.

The Experimental layer is where the user defines their code for running their experiments. This will create an instance of the Manager class defined in the Core layer which allows the user access to the hardware of the system. The Experimental layer is split into two sub-layers, Base and Execution. The Base sub-layer is a class which defines a series of methods that are common to each experiment that the user will perform. This is where the user instantiates the Manager class from the Core layer of the system. The Execution layer is a child class of the Base. The user defines a series of methods that are specific to each experimental run. They provide a series of experimental parameters for the Execution to parse and perform. For example, this could be a series of reagent volumes in .CSV or .JSON format. This approach (Fig. 1.10) allows the user to define a core set of operations for each experiment in a single parent class and specific operations as a child, preventing the duplication of code across several different experiments.

1.3.4 Analytical layer

The Analytical layer is an optional, stand-alone layer which runs independently from the other layers of this architecture. Whilst user can use this design to conduct experiments and gather data alone, the Analytical layer gives the user the option of processing their data to gather valuable insights. The main purpose of this layer is to house several algorithms and analytical tools the user wishes to use to process

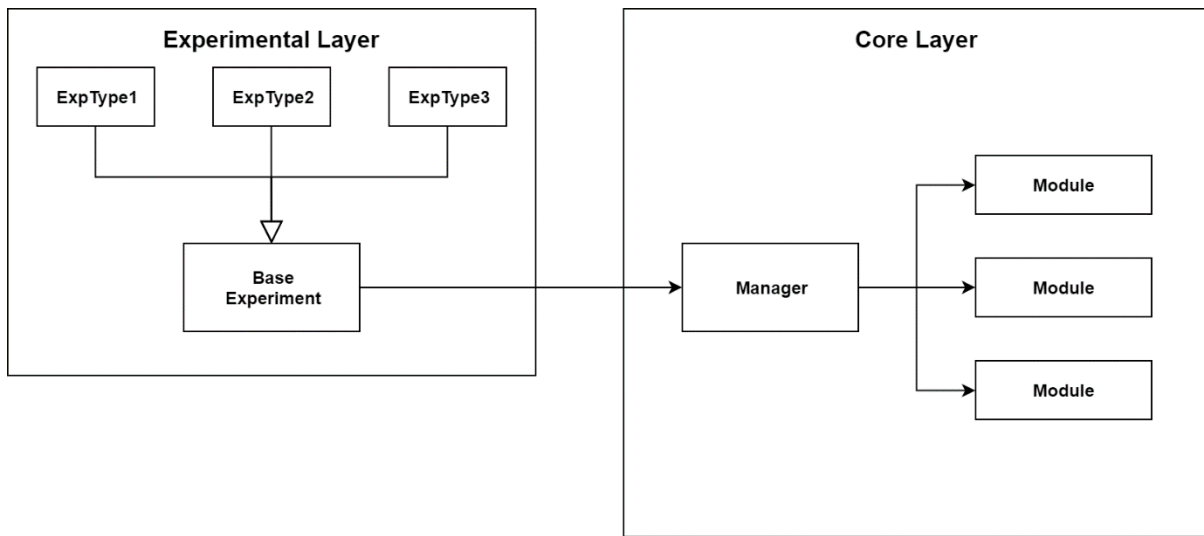


Figure 1.10. Outline of how the Experimental Layer interacts with the Core Layer of the system. The Base Experiment creates an instance of the Manager class in the Core Layer which allows the experiments to interface with the hardware of the system.

their data. The ideal workflow, outlined in Figure 1.8, is for the platform to generate data from experiments and the Analytical layer to process this data in order to generate new experimental parameters and/or a series of other tasks. For example, training of a machine learning classifier, optimisation of experimental conditions via genetic algorithms, or simple data processing tasks.

1.3.5 Digital code

Figure 1.11 shows the general concept of abstraction of inorganic synthesis into digital code for use on automated systems.

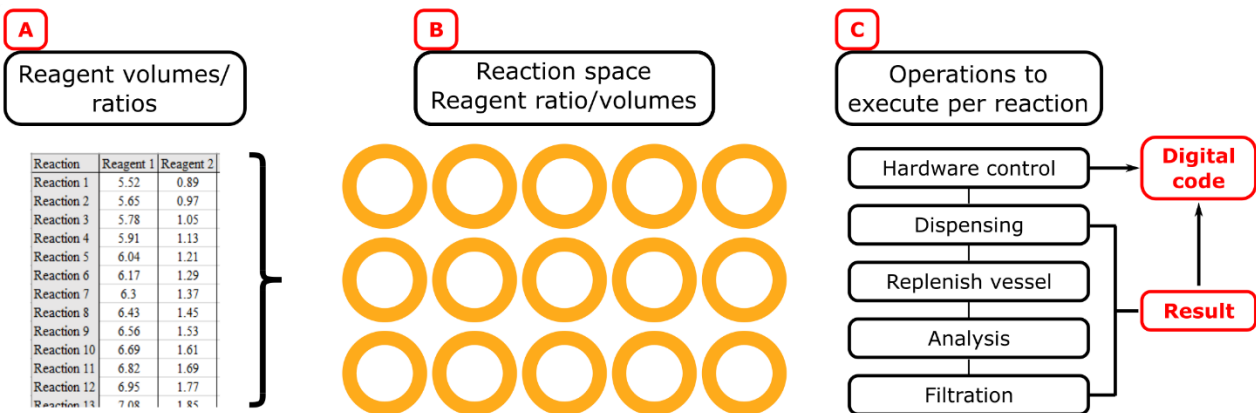


Figure 1.11 A) Table format of desired reaction volumes and reagent ratios. B) Extraction of the data contained in A into individual reaction files. C) Execution of the desired reactions on a given hardware workflow to complete the digital synthesis code.

Figure 1.12 shows the specific instantiation on our system, of the concept shown above, for the synthesis of inorganic clusters

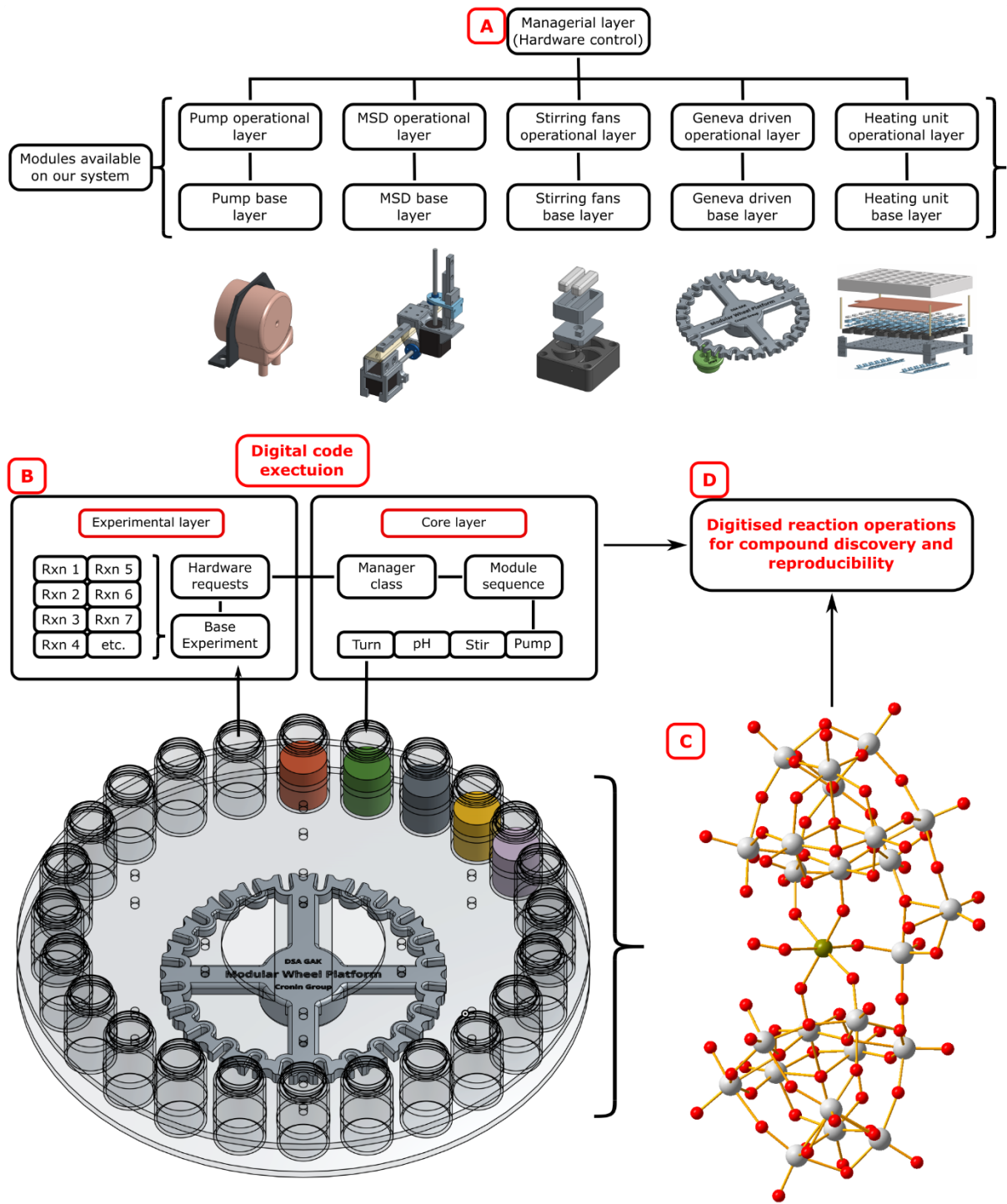


Figure 1.12 A) Hardware modules available to the system of this work. B) Workflow being performed on the platform by the experimental and core layer code described above. C) Reaction resulting in new discovery. D) Result combined with the code to operate the hardware forming digital synthetic code.

2. Experimental

2.1 Reaction conditions and chemical Space 1 and 2

2.1.1 Space 1 stock solutions and reactions:

- Sodium tungstate dihydrate $\text{Na}_2\text{WO}_4 \cdot 2\text{H}_2\text{O}$ [0.66 M] adjusted to pH 3 using conc. HCl in H_2O (Sigma Aldrich ACS reagent, $\geq 99\%$)
- Dimethylamine hydrochloride $(\text{CH}_3)_2\text{NH} \cdot \text{HCl}$ [2.45 M] in H_2O (Sigma Aldrich, $\geq 99\%$)
- Sodium Dithionite $\text{Na}_2\text{S}_2\text{O}_4$ [0.5 M] H_2O (Sigma Aldrich technical grade, $\geq 85\%$)
- Hydrochloric acid [0.5 M] (Sigma Aldrich ACS reagent)
- Cobalt chloride hexahydrate, $\text{CoCl}_2 \cdot 6\text{H}_2\text{O}$ [0.5 M] (Sigma Aldrich ACS reagent, $\geq 99\%$)
- Nickel chloride hexahydrate, $\text{NiCl}_2 \cdot 6\text{H}_2\text{O}$ [0.5 M] (Sigma Aldrich ACS reagent, $\geq 99.9\%$)
- Manganese chloride tetrahydrate, $\text{MnCl}_2 \cdot 4\text{H}_2\text{O}$ [0.5 M] (Sigma Aldrich ACS reagent, $\geq 98\%$)
- Iron chloride tetrahydrate, $\text{FeCl}_2 \cdot 4\text{H}_2\text{O}$ [0.5 M] (Sigma Aldrich ACS reagent, $\geq 99\%$)

Reactions from which the analysed samples of compounds **1-3** were originally found are highlighted in red. These conditions were repeated many times to determine reproducibility of the compounds.

Space 1 (Compounds **[1]** [**2**] and **[3]**) (All values in mL):

Rxn	W	DMA	Thionite	Acid	Co	Ni	Mn	Fe	Total rxn
1	5.0000	4.0000	0.7300	0.1000	0.4250	0.0000	0.0000	0.0000	10.255
2	5.0000	4.0000	0.7300	0.1000	0.3750	0.0250	0.0000	0.0000	10.230
3	5.0000	4.0000	0.7300	0.1000	0.3250	0.0750	0.0000	0.0000	10.230
4	5.0000	4.0000	0.7300	0.1000	0.2750	0.1250	0.0000	0.0000	10.230
5	5.0000	4.0000	0.7300	0.1000	0.2250	0.1750	0.0000	0.0000	10.230
6	5.0000	4.0000	0.7300	0.1000	0.1750	0.2250	0.0000	0.0000	10.230
7	5.0000	4.0000	0.7300	0.1000	0.1250	0.2750	0.0000	0.0000	10.230
8	5.0000	4.0000	0.7300	0.1000	0.0750	0.3250	0.0000	0.0000	10.230
9	5.0000	4.0000	0.7300	0.1000	0.0250	0.3750	0.0000	0.0000	10.230
10	5.0000	4.0000	0.7300	0.1000	0.0000	0.4250	0.0000	0.0000	10.255
11	5.0000	4.0000	0.7300	0.1000	0.3375	0.0000	0.0875	0.0000	10.255
12	5.0000	4.0000	0.7300	0.1000	0.3000	0.0375	0.0750	0.0000	10.243
13	5.0000	4.0000	0.7300	0.1000	0.2625	0.0750	0.0625	0.0000	10.230
14	5.0000	4.0000	0.7300	0.1000	0.2250	0.1125	0.0500	0.0125	10.230
15	5.0000	4.0000	0.7300	0.1000	0.1875	0.1500	0.0375	0.0250	10.230
16	5.0000	4.0000	0.7300	0.1000	0.1500	0.1875	0.0250	0.0375	10.230
17	5.0000	4.0000	0.7300	0.1000	0.1125	0.2250	0.0125	0.0500	10.230
18	5.0000	4.0000	0.7300	0.1000	0.0750	0.2625	0.0000	0.0625	10.230
19	5.0000	4.0000	0.7300	0.1000	0.0375	0.3000	0.0000	0.0750	10.243
20[3]	5.0000	4.0000	0.7300	0.1000	0.0000	0.3375	0.0000	0.0875	10.255
21	5.0000	4.0000	0.7300	0.1000	0.2500	0.0250	0.1750	0.0063	10.286
22[2]	5.0000	4.0000	0.7300	0.1000	0.2250	0.0500	0.1563	0.0250	10.286

23	5.0000	4.0000	0.7300	0.1000	0.2000	0.0750	0.1375	0.0438	10.286
24	5.0000	4.0000	0.7300	0.1000	0.1750	0.1000	0.1188	0.0625	10.286
25	5.0000	4.0000	0.7300	0.1000	0.1500	0.1250	0.1000	0.0813	10.286
26	5.0000	4.0000	0.7300	0.1000	0.1250	0.1500	0.0813	0.1000	10.286
27	5.0000	4.0000	0.7300	0.1000	0.1000	0.1750	0.0625	0.1188	10.286
28	5.0000	4.0000	0.7300	0.1000	0.0750	0.2000	0.0438	0.1375	10.286
29	5.0000	4.0000	0.7300	0.1000	0.0500	0.2250	0.0250	0.1563	10.286
30	5.0000	4.0000	0.7300	0.1000	0.0250	0.2500	0.0063	0.1750	10.286
31	5.0000	4.0000	0.7300	0.1000	0.1625	0.0500	0.2625	0.0000	10.305
32	5.0000	4.0000	0.7300	0.1000	0.1500	0.0625	0.2313	0.0125	10.286
33	5.0000	4.0000	0.7300	0.1000	0.1375	0.0750	0.2000	0.0438	10.286
34	5.0000	4.0000	0.7300	0.1000	0.1250	0.0875	0.1688	0.0750	10.286
35	5.0000	4.0000	0.7300	0.1000	0.1125	0.1000	0.1375	0.1063	10.286
36	5.0000	4.0000	0.7300	0.1000	0.1000	0.1125	0.1063	0.1375	10.286
37	5.0000	4.0000	0.7300	0.1000	0.0875	0.1250	0.0750	0.1688	10.286
38	5.0000	4.0000	0.7300	0.1000	0.0750	0.1375	0.0438	0.2000	10.286
39	5.0000	4.0000	0.7300	0.1000	0.0625	0.1500	0.0125	0.2313	10.286
40	5.0000	4.0000	0.7300	0.1000	0.0500	0.1625	0.0000	0.2625	10.305
41	5.0000	4.0000	0.7300	0.1000	0.0750	0.0188	0.3500	0.0125	10.286
42	5.0000	4.0000	0.7300	0.1000	0.0688	0.0250	0.3125	0.0500	10.286
43	5.0000	4.0000	0.7300	0.1000	0.0625	0.0313	0.2750	0.0875	10.286
44	5.0000	4.0000	0.7300	0.1000	0.0563	0.0375	0.2375	0.1250	10.286
45	5.0000	4.0000	0.7300	0.1000	0.0500	0.0438	0.2000	0.1625	10.286
46	5.0000	4.0000	0.7300	0.1000	0.0438	0.0500	0.1625	0.2000	10.286
47	5.0000	4.0000	0.7300	0.1000	0.0375	0.0563	0.1250	0.2375	10.286
48	5.0000	4.0000	0.7300	0.1000	0.0313	0.0625	0.0875	0.2750	10.286
49	5.0000	4.0000	0.7300	0.1000	0.0250	0.0688	0.0500	0.3125	10.286
50	5.0000	4.0000	0.7300	0.1000	0.0188	0.0750	0.0125	0.3500	10.286
51	5.0000	4.0000	0.7300	0.1000	0.0000	0.0000	0.4250	0.0875	10.343
52	5.0000	4.0000	0.7300	0.1000	0.0000	0.0000	0.3875	0.1250	10.343
53	5.0000	4.0000	0.7300	0.1000	0.0000	0.0000	0.3500	0.1625	10.343
54	5.0000	4.0000	0.7300	0.1000	0.0000	0.0000	0.3125	0.2000	10.343
55	5.0000	4.0000	0.7300	0.1000	0.0000	0.0000	0.2750	0.2375	10.343
56	5.0000	4.0000	0.7300	0.1000	0.0000	0.0000	0.2375	0.2750	10.343
57	5.0000	4.0000	0.7300	0.1000	0.0000	0.0000	0.2000	0.3125	10.343
58	5.0000	4.0000	0.7300	0.1000	0.0000	0.0000	0.1625	0.3500	10.343
59	5.0000	4.0000	0.7300	0.1000	0.0000	0.0000	0.1250	0.3875	10.343
60[1]	5.0000	4.0000	0.7300	0.1000	0.0000	0.0000	0.3500	10.343	

2.1.2 Space 2 stock solutions and reactions

- Sodium tungstate dihydrate Na₂WO₄.2H₂O [0.66 M] adjusted to pH 3 using conc HCl in H₂O (Sigma Aldrich ACS reagent, ≥99%)
- Dimethylamine hydrochloride (CH₃)₂NH.HCl [2.453 M] in H₂O (Sigma Aldrich, ≥99%)
- Sodium Dithionite Na₂S₂O₄ [0.5 M] H₂O (Sigma Aldrich technical grade, ≥85%)
- Hydrochloric acid [0.5 M] (Sigma Aldrich ACS reagent)
- Vanadium dichloride, VCl₂ [0.5 M] (Sigma Aldrich, 85%)

Reactions from which compound **4** was found highlighted in red

Space 2 (Compound **[4]**) (All values in mL):

Rxn	W	DMA	Thionite	Acid	V	Total rxn
1	5.000	4.000	0.730	0.100	0.350	10.180
2	5.000	4.000	0.730	0.100	0.350	10.180
3	5.000	4.000	0.730	0.100	0.350	10.180
4	5.000	4.000	0.730	0.100	0.350	10.180
5	5.000	4.000	0.730	0.100	0.350	10.180
6	5.000	4.000	0.730	0.100	0.350	10.180
7 [4]	5.000	4.000	0.730	0.100	0.500	10.330
8 [4]	5.000	4.000	0.730	0.100	0.650	10.480
9 [4]	5.000	4.000	0.730	0.100	0.800	10.630
10	5.000	4.000	0.730	0.100	1.250	11.080
11	5.000	4.000	0.730	0.100	1.400	11.230
12	5.000	4.000	0.730	0.100	1.550	11.380
13	5.000	4.000	0.730	0.100	1.700	11.530
14	5.000	4.000	0.730	0.100	1.850	11.680
15	5.000	4.000	0.730	0.000	0.500	10.230
16	5.000	4.000	0.730	0.000	0.650	10.380
17	5.000	4.000	0.730	0.000	0.800	10.530
18	5.000	4.000	0.730	0.000	0.950	10.680
19	5.000	4.000	0.730	0.000	1.100	10.830
20	5.000	4.000	0.730	0.000	1.250	10.980
21	5.000	4.000	0.730	0.000	1.400	11.130
22	5.000	4.000	0.730	0.000	1.550	11.280
23	5.000	4.000	0.730	0.000	1.700	11.430
24	5.000	4.000	0.730	0.000	1.850	11.580

2.1.3 Reaction details

In all cases the reactants were dispensed in immediate succession in the order below:

1. Tungstate/DMA
2. Acid
3. Thionite
4. Transition metal 1-4

This order of addition, timing and vial size has proven crucial to the formation of the products described in this work. In the case of compound [1] the persistence of the deep blue solution colour for several days (4-5 days minimum is ideal) is the key to recognizing a successful reaction. All other compounds have this same colour change but will fade after approximately 2 h. Addition of the FeCl₂ solution immediately following the reducing agent is crucial here. All reactions were stirred at ca 800 rpm for 1-2 h in a 14 mL disposable glass vial and vacuum filtered using the filtration array described above through PTFE frits + filter paper. Crystallization times varied from 1 week to >2 months. Crystallography data recorded on a Bruker Apex diffractometer. All IR spectra were run on solid isolated powder.

2.1.4 (C₂H₈N)₁₀Na₂[H₆Fe(O₂)W₂₄O₈₂(H₂O)₂₅] (1, {W₂₄Fe}) – Initial Discovery

Under stirring aqueous sodium tungstate (5 mL, Na₂WO₄.2H₂O, [0.66 M], Adjusted to pH 3) stock solution was dispensed into a 14 mL vial. Aqueous dimethylamine hydrochloride (4 mL, (CH₃)₂NH.HCl [2.453 M]) was added. Hydrochloric acid [0.1 mL, 0.5 M] added. Aqueous sodium dithionite (0.73 mL, Na₂S₂O₄ [0.5 M]) was added, colour change from clear to deep blue occurred immediately upon addition. Finally, aqueous iron chloride tetrahydrate (0.35 mL, FeCl₂.4H₂O [0.5 M]) was added. The reaction was left stirring at RT for 1 hour. The reaction mixed remained blue for approx. 5 days and was then filtered through standard Whatman filter paper via the filtration array (SI section 1.2.7) and left to crystallize in an open 14 mL vial. After 4-weeks pale yellow crystals were obtained (SI section 2.5 A and G).

Average yield across 5 repeat reactions: 0.104 g (9% based on W); yellow block crystals; Triclinic; space group *P*-1, $M_r = 6685.53 \text{ g}\cdot\text{mol}^{-1}$, $a = 13.1545(16)$, $b = 18.807(2)$, $c = 25.522(3) \text{ \AA}$, $\alpha = 104.421(2)$, $\beta = 104.482(2)$, $\gamma = 96.678(2)^\circ$; $V = 5812.3(12) \text{ \AA}^3$, $Z = 2$; $\rho = 3.820 \text{ Mg}\cdot\text{m}^{-3}$, $\lambda(\text{Mo-K}\alpha) = 0.71073 \text{ \AA}$, 197690 Reflections measured, 22842 unique reflections [$R_{(\text{int})} = 0.0365$] which were used in all calculations, 1379 refined parameters, final $RI = 0.0300$ and $wR2 = 0.0711$ (all data); Characteristic FT-IR bands (cm⁻¹); 1580 (b), 1460 (w), 1413 (w), 1016 (w), 937 (s), 875 (m), 501 (w); Raman O-O superoxide peak 967 cm⁻¹ (s); Elemental analysis Calculated (%) W(65.88), Fe(0.87), C(3.59), H(1.9), N(2.11) Found (%) W(65.58), Fe(0.92), C(4.06), H(1.81), N(2.28).

2.1.5 (C₂H₈N)₁₀Na₂[H₆Fe(O₂)W₂₄O₈₂(H₂O)₂₅] (1, {W₂₄Fe}) – Reproduction, fresh reagents

Under stirring aqueous sodium tungstate (5 mL, Na₂WO₄.2H₂O, [0.66 M], Adjusted to pH 3) stock solution was dispensed into a 14 mL vial. Aqueous dimethylamine hydrochloride (4 mL, [2.453 M])

was added. Hydrochloric acid [0.1 mL, 0.5 M] added. An aqueous solution of freshly purchased sodium dithionite (0.1 mL, Na₂S₂O₄ [0.5 M]) was added, colour change from clear to deep blue occurred immediately upon addition. Finally, a green solution of freshly purchased aqueous iron(II)chloride tetrahydrate (0.1 mL, FeCl₂.4H₂O [0.5 M]) was added. The reaction was left stirring at RT for 2 hours. The reaction mixed was then filtered through a 0.45 µm syringe filter after 5 days and left to crystalize in an open 14 mL vial. The solution remained dark for approx. 20 days and after 3-weeks colourless crystals were obtained which matched those found in SI Section 2.1.4.

2.1.6 (C₂H₈N)₇₂Na₁₆[H₁₆Co₈W₂₀₀O₆₆₀(H₂O)₄₀]·600H₂O (2, {W₂₀₀Co₈}),

Under stirring aqueous sodium tungstate (5 mL, Na₂WO₄.2H₂O, [0.66 M], Adjusted to pH 3) stock solution was dispensed into a 14 mL vial. Aqueous dimethylamine hydrochloride (4 mL, (CH₃)₂NH.HCl [2.453 M]) was added. Hydrochloric acid [0.1 mL, 0.5 M] added. Aqueous sodium dithionite (0.73 mL, Na₂S₂O₄ [0.5 M]) was added, colour change from clear to deep blue occurred immediately upon addition. Finally, transition metal solutions were added in the following order; aqueous cobalt chloride hexahydrate (0.225 mL, CoCl₂.6H₂O [0.5 M]), aqueous nickel chloride hexahydrate (0.05mL, NiCl₂.6H₂O, [0.5 M]), aqueous manganese chloride tetrahydrate (0.1563 mL, MnCl₂.4H₂O, [0.5 M]) and aqueous iron chloride tetrahydrate (0.025 mL, FeCl₂.4H₂O, [0.5 M]). The reaction was left stirring at RT for 1 hour. The reaction mixed remained blue for approx. 30-45 minutes and was then filtered through standard Whatman filter paper via the filtration array (SI section 1.2.7) and left to crystalize in an open 14 mL vial. After 5-8 weeks red serrated star shape crystals (SI section 2.5 B, E, F and H).were obtained which were found to correspond to those previously reported by our group (CSD 895471).^[5]

Characteristic FT-IR bands (cm⁻¹); 1582(b), 1440 (m), 978(w), 898(w), 842(m), 503(w)

2.1.7 (C₂H₈N)₇₂Na₁₆[H₁₆Ni₈W₂₀₀O₆₆₀(H₂O)₄₀]·360H₂O (3, {W₂₀₀Ni₈})

Under stirring aqueous sodium tungstate (5 mL, Na₂WO₄.2H₂O, [0.66 M], Adjusted to pH 3) stock solution was dispensed into a 14mL vial. Aqueous dimethylamine hydrochloride (4 mL, (CH₃)₂NH.HCl [2.453 M]) was added. Hydrochloric acid [0.1 mL, 0.5 M] added. Aqueous sodium dithionite (0.73 mL, Na₂S₂O₄ [0.5 M]) was added, colour change from clear to deep blue occurred immediately upon addition. Finally, transition metal solutions were added in the following order; aqueous nickel chloride hexahydrate (03375mL, NiCl₂.6H₂O, [0.5 M]), aqueous iron chloride tetrahydrate (0.0875 mL, FeCl₂.4H₂O, [0.5 M]). The reaction was left stirring at RT for 1 hour. The reaction mixed remained blue for approx. 30-45 minutes and was then filtered through standard Whatman filter paper via the filtration array (SI section 1.2.7) and left to crystalize in an open 14 mL vial. After 8-10 weeks yellow serrated star shape crystals were obtained (SI section 2.5 images C and I).

Average yield across 5 repeat reactions 9 mg (0.45 % based on W); Yellow serrated star shaped crystals (see SI section 2.5 Crystal images); Tetragonal space group *P42/nmc*, *a* = 48.8657(4), *c* = 29.4123(2) Å; *V* = 70232.4(7) Å³; *Z* = 2; *ρ* = 2.786 Mg·m⁻³; *λ*(Mo-Kα = 0.71073 Å. 383669 reflections measured; 33492 unique reflections [*R*_(int) = 0.0711] which were used in all calculations; 1132 refined parameters;

final $RI = 0.0677$ and $wR2 = 0.195$ (all data); Characteristic FT-IR (powder) bands (cm^{-1}); 1595 (b), 1462 (m), 972 (w), 929 (w), 848 (m), 501 (w); Elemental analysis Calculated (%) W(60.94), Ni(0.778), C(2.86), H(2.62), N(1.67) Found (%) W(63.02), Ni(0.765), C(3.3), H(1.45), N(1.63).

2.1.8 $(\text{C}_2\text{H}_8\text{N})_{14}[\text{H}_{26}\text{W}_{34}\text{V}_4\text{O}_{130}](\text{H}_2\text{O})_{32}$ (4, $\{\text{W}_{34}\text{V}_4\}$),

Under stirring aqueous sodium tungstate (5 mL, $\text{Na}_2\text{WO}_4 \cdot 2\text{H}_2\text{O}$, [0.66 M], Adjusted to pH 3) stock solution was dispensed into a 14mL vial. Aqueous dimethylamine hydrochloride (4 mL, $(\text{CH}_3)_2\text{NH} \cdot \text{HCl}$ [2.453 M]) was added. Hydrochloric acid [0.1 mL, 0.5 M] added. Aqueous sodium dithionite (0.73 mL, $\text{Na}_2\text{S}_2\text{O}_4$ [0.5 M]) was added, colour change from clear to deep blue occurred immediately upon addition. Finally, fresh aqueous vanadium dichloride (0.65 mL, VCl_2 [0.5 M]) was added, colour change to deep blue/black was observed upon addition. The reaction was left stirring at RT for 1 hour. The reaction solution remained blue/black indefinitely and was then filtered through standard Whatman filter paper via the filtration array (SI section 1.2.7) and left to crystallize in an open 14 mL vial. After 4-weeks black needles crystals were obtained (SI section 2.5 D and J).

Average yield across 5 repeat reactions 14 mg (0.74 % based on W); Black needle crystals; Triclinic space group $P-1$, $a = 13.5219(16)$, $b = 18.592(2)$, $c = 20.285(2)$ Å, $\alpha = 68.689(2)$, $\beta = 79.219(2)$, $\gamma = 75.283(2)^\circ$; $V = 4569.5(9)$ Å³; $Z = 1$; $\rho = 3.555 \text{ Mg} \cdot \text{m}^{-3}$; 57247 Reflections measured; 17941 unique reflections [$R_{(\text{int})} = 0.0516$] which were used in all calculations; 976 refined parameters; final $RI = 0.0421$ and $wR2 = 0.1197$ (all data); Characteristic FT-IR bands (cm^{-1}); 1584 (b), 1462 (s), 982 (w), 941 (s), 838 (m), 745 (w), 578 (w); Elemental analysis Calculated (%) W(62.18), V(2.03), C(3.52), H(1.75), N(2.05) Found (%) W(61.67), V(2.114), C(3.91), H(1.4), N(2.14).

2.2 Crystallography and crystal data

2.2.1 Crystallography

Suitable single crystals were selected and mounted onto a rubber loop using Fomblin oil. X-ray diffraction intensity data was collected on a Bruker Apex Quasar CCD diffractometer (λ (MoK α) = 0.71073 Å) equipped with a microfocus x-ray source (50 kV, 1.00 mA) or a Rigaku XtaLAB Synergy R HyPix-Arc HPC diffractometer (λ (MoK α) = 0.71073 Å) equipped with a rotating anode X-ray source (50 kV, 24.00 mA). Data collection and reduction were performed using the Apex2 or CrysAlisPro software package and structure solution, and refinement were carried out using SHELXS-97^[1] and SHELXL-97^[2] using WinGX suite.^[3] Corrections for incident and diffracted beam absorption effects were applied using empirical absorption correction.^[4] Most of the non-hydrogen atoms (including those disordered) were anisotropically refined. CCDC 1972365-1972367 contain the supplementary crystallographic data for compounds **1**, **3** and **4**. These data can be obtained free of charge via www.ccdc.cam.ac.uk/data_request/cif, or by emailing data_request@ccdc.cam.ac.uk, or by contacting The Cambridge Crystallographic Data Centre, 12 Union Road, Cambridge CB2 1EZ, UK; fax: +44 1223 336033.

Reference

- [1] G. Sheldrick, *Acta. Crystallogr. A* **1990**, *46*, 467-473
- [2] G. Sheldrick, *Acta. Crystallogr. A* **2008**, *64*, 112-122
- [3] L. Farrugia, *J. Appl. Crystallogr.* **1999**, *32*, 837-838
- [4] R. C. Clark, J. S. Reid, *Acta. Crystallogr. A* **1995**, *51*, 887-897
- [5] L. Cronin et al., *Angew. Chem. Int. Ed.*, **2012**, *51*, 12759-12762

2.2.2 Crystal data

Table 1. Crystal data and structure refinement for compound [1].

Empirical formula	$C_{20}H_{126}FeN_{10}Na_2O_{104}W_{24}$	
Formula weight	6685.53	
Temperature	150(2) K	
Wavelength	0.71073 Å	
Crystal system	Triclinic	
Space group	P -1	
Unit cell dimensions	$a = 13.1545(16)$ Å	$\alpha = 104.421(2)^\circ$.
	$b = 18.807(2)$ Å	$\beta = 104.482(2)^\circ$.
	$c = 25.522(3)$ Å	$\gamma = 96.678(2)^\circ$.
Volume	$5812.3(12)$ Å ³	
Z	2	
Density (calculated)	3.820 Mg/m ³	
Absorption coefficient	23.881 mm ⁻¹	
F(000)	5944	
Crystal size	0.168 x 0.122 x 0.060 mm ³	
Theta range for data collection	1.139 to 26.000°.	
Index ranges	$-16 \leq h \leq 16, -23 \leq k \leq 23, -31 \leq l \leq 31$	
Reflections collected	197690	
Independent reflections	22842 [R(int) = 0.0365]	
Completeness to theta = 25.242°	100.0 %	
Absorption correction	Empirical	
Max. and min. transmission	0.0338 and 0.0028	
Refinement method	Full-matrix least-squares on F ²	
Data / restraints / parameters	22842 / 67 / 1379	
Goodness-of-fit on F ²	1.108	
Final R indices [I>2sigma(I)]	R1 = 0.0300, wR2 = 0.0711	
R indices (all data)	R1 = 0.0338, wR2 = 0.0738	
Extinction coefficient	n/a	
Largest diff. peak and hole	2.74 and -2.66 e.Å ⁻³	

Table 2. Crystal data and structure refinement for compound [3].

Empirical formula	C ₁₄₄ H ₁₅₇₂ N ₇₂ Na ₁₆ Ni ₈ O ₁₁₅₀ W ₂₀₀	
Formula weight	60330.16	
Temperature	150(2) K	
Wavelength	0.71073 Å	
Crystal system	Tetragonal	
Space group	P 42/n m c	
Unit cell dimensions	a = 48.8657(2) Å	a= 90°.
	b = 48.8657(2) Å	b= 90°.
	c = 29.4123(2) Å	g = 90°.
Volume	70232.4(7) Å ³	
Z	2	
Density (calculated)	2.853 Mg/m ³	
Absorption coefficient	16.516 mm ⁻¹	
F(000)	54680	
Crystal size	0.114 x 0.086 x 0.076 mm ³	
Theta range for data collection	2.277 to 25.499°.	
Index ranges	-59<=h<=49, -59<=k<=50, -33<=l<=35	
Reflections collected	383669	
Independent reflections	33492 [R(int) = 0.0711]	
Completeness to theta = 25.242°	99.9 %	
Absorption correction	Gaussian	
Max. and min. transmission	0.488 and 0.311	
Refinement method	Full-matrix least-squares on F ²	
Data / restraints / parameters	33492 / 46 / 1132	
Goodness-of-fit on F ²	1.134	
Final R indices [I>2sigma(I)]	R1 = 0.0677, wR2 = 0.1524	
R indices (all data)	R1 = 0.1129, wR2 = 0.1950	
Extinction coefficient	n/a	
Largest diff. peak and hole	2.848 and -2.255 e.Å ⁻³	

Table 3. Crystal data and structure refinement for compound [4].

Empirical formula	C ₂₈ H ₂₀₂ N ₁₄ O ₁₆₂ V ₄ W ₃₄	
Formula weight	9782.68	
Temperature	150(2) K	
Wavelength	0.71073 Å	
Crystal system	Triclinic	
Space group	P -1	
Unit cell dimensions	a = 13.5219(16) Å	a = 68.689(2)°.
	b = 18.592(2) Å	b = 79.219(2)°.
	c = 20.285(2) Å	g = 75.283(2)°.
Volume	4569.5(9) Å ³	
Z	1	
Density (calculated)	3.555 Mg/m ³	
Absorption coefficient	21.604 mm ⁻¹	
F(000)	4372	
Crystal size	0.100 x 0.100 x 0.050 mm ³	
Theta range for data collection	1.566 to 26.000°.	
Index ranges	-16<=h<=16, -22<=k<=22, -25<=l<=25	
Reflections collected	57247	
Independent reflections	17941 [R(int) = 0.0516]	
Completeness to theta = 25.242°	99.9 %	
Absorption correction	Empirical	
Max. and min. transmission	0.493 and 0.308	
Refinement method	Full-matrix least-squares on F ²	
Data / restraints / parameters	17941 / 23 / 976	
Goodness-of-fit on F ²	1.090	
Final R indices [I>2sigma(I)]	R1 = 0.0421, wR2 = 0.0995	
R indices (all data)	R1 = 0.0682, wR2 = 0.1197	
Extinction coefficient	n/a	
Largest diff. peak and hole	3.09 and -2.69 e.Å ⁻³	

2.3 Compound [1] IR and Raman data

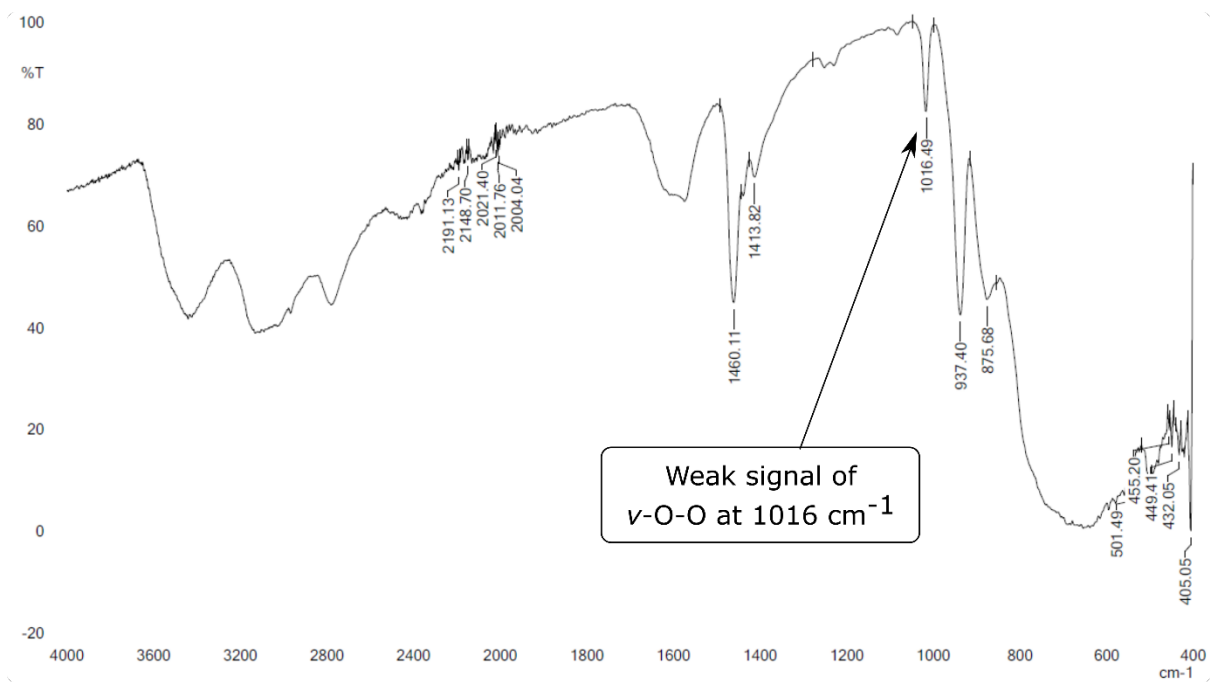


Figure 2.1 IR spectrum of [1] W₂₄Fe-superoxide

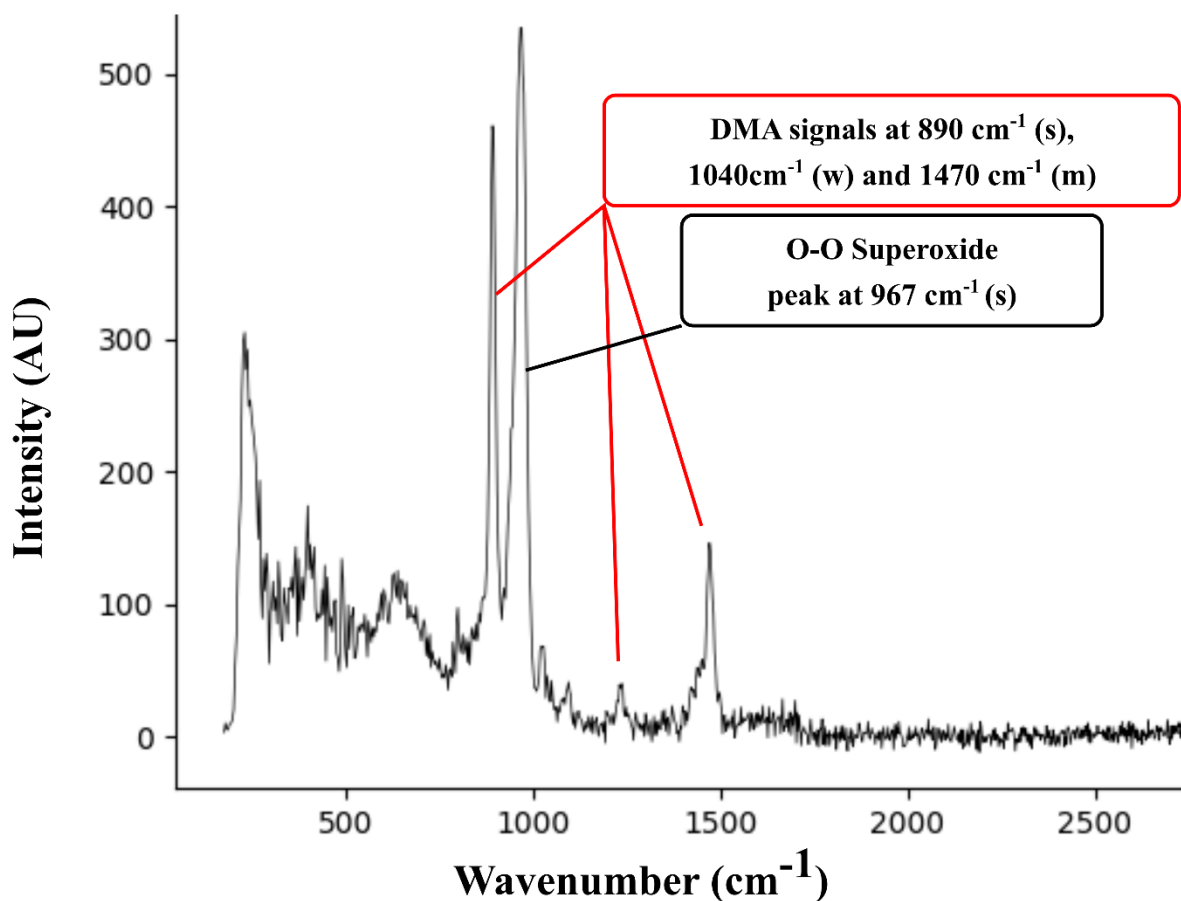


Figure 2.4 Raman spectrum of [1] W₂₄Fe-superoxide

2.4 Compound [1] Evans Method NMR and U_{eff}

Evans method NMR using water as the reference solvent (Figure 2.3).

Sample weight of 7.5 mg (0.00186 mmol)

Shift of 67.353 ppm yields an effective magnetic moment of 5.832. Fe^{3+} high spin.

Measurement recorded using a Bruker 600 MHz spectrometer

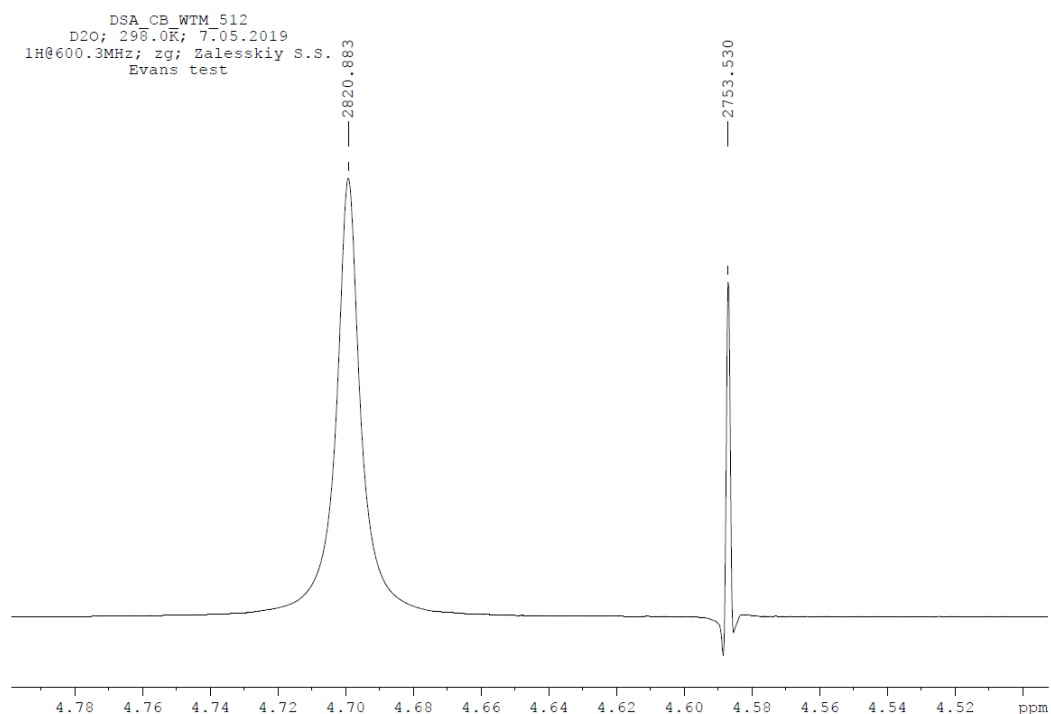


Figure 2.3 ¹H NMR spectra by Evans method for compounds 3 (W_{24}Fe -superoxide)

2.5 Crystal images

Images of the crystal populations of compounds [1-4] as well as examples of the multiple species being produced from single reactions are included in figure 2.5.

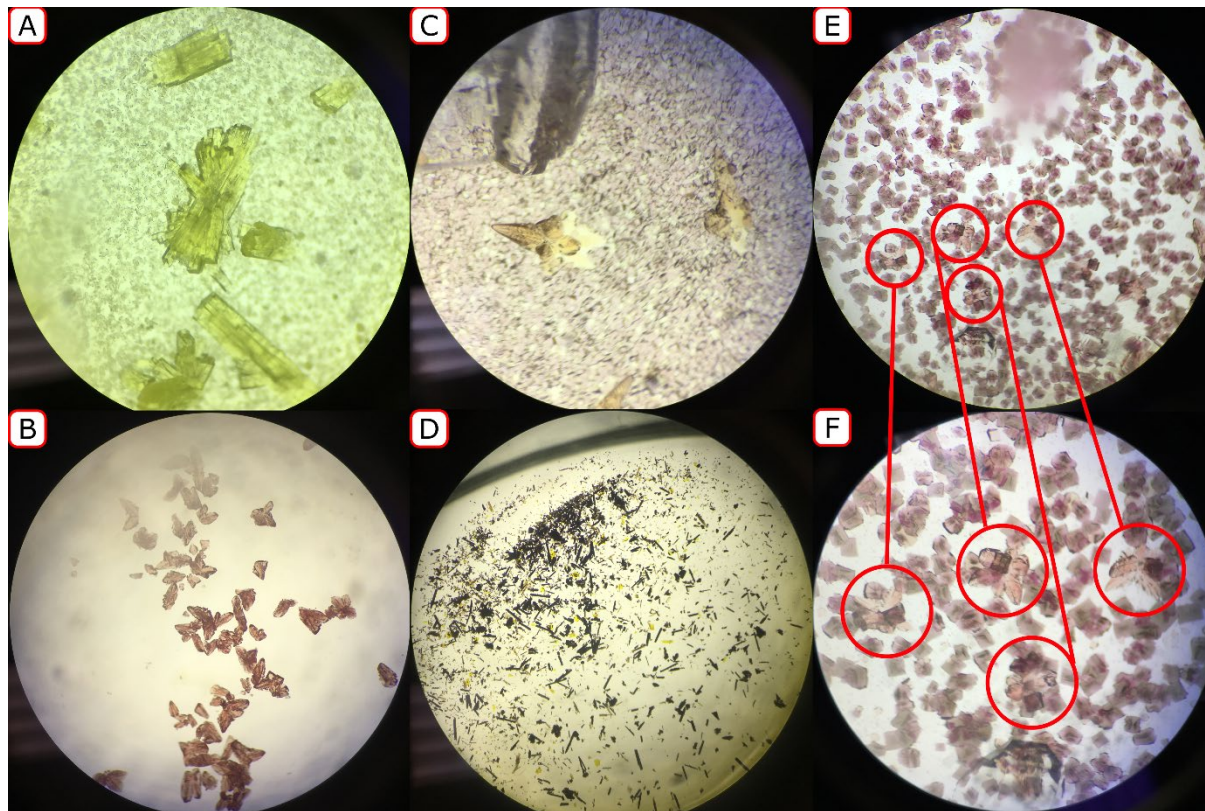


Figure 2.5 **Image A-** Yellow cuboid plate crystals of W_{24}Fe -superoxide [1] formed in large discrete assemblies. **Image B-** Red serrated star shaped crystals of $\text{W}_{200}\text{Co}_8$ [2] forming as the single species in reaction 22 (section 2.1.1). **Image C-** Yellow distorted serrated star shaped crystals of $\text{W}_{200}\text{Ni}_8$ forming on a bed of unreacted Na_2WO_4 crystals (confirmed by unit cell check). **Image D-** Black cuboid crystals of W_{34}V_4 [4]. **Image E + F-** As mentioned in the manuscript, some of the reactions that produced W_{200}M_8 formed other species in the same reaction vial due to the long crystallisation period required for this large cluster to form. These sample images show numerous well formed W_{200}M_8 crystals amongst other POM species, in this case a simple known W_{11}Co Keggan cluster (confirmed by x-ray crystallography). This phenomenon should be expected in many cases when attempting to reproduce this work.

Close detail images of each crystal types are included in Figure 2.6.

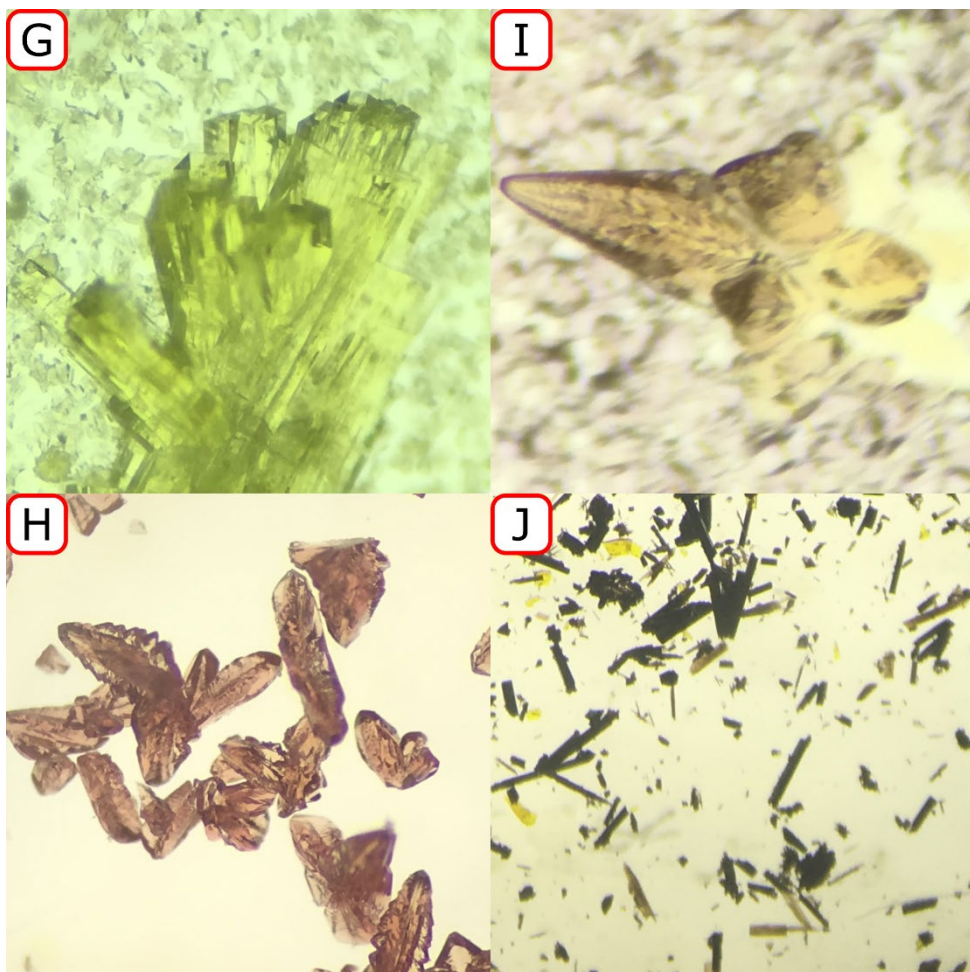


Figure 2.6 **Image G-** Detailed image of a single assembly of yellow cuboid plate crystals of W_{24}Fe -superoxide [1]. **Image H-** Detailed image of red serrated star shaped crystals of $\text{W}_{200}\text{Co}_8$ [2] forming as the single species in reaction 22 (section 2.1.1). **Image I-** Detailed image of yellow distorted serrated star shaped crystal of $\text{W}_{200}\text{Ni}_8$. **Image J-** Detailed image of black cuboid crystals of W_{34}V_4 [4].